© 2018. Published by The Company of Biologists Ltd | Journal of Cell Science (2018) 131, jcs214775. doi:10.1242/jcs.214775

RESEARCH ARTICLE

Parallel signaling pathways regulate excitable dynamics differently to mediate pseudopod formation during eukaryotic chemotaxis

Yuki Tanabe[1,2], Yoichiro Kamimura[2,*] and Masahiro Ueda[1,2,3,*]

ABSTRACT

In eukaryotic chemotaxis, parallel signaling pathways regulate the spatiotemporal pseudopod dynamics at the leading edge of a motile cell through the characteristic dynamics of an excitable system; however, differences in the excitability and the physiological roles of individual pathways remain to be elucidated. Here, we found that two different pathways, mediated by soluble guanylyl cyclase (sGC) and phosphoinositide 3-kinase (PI3K), caused similar all-or-none responses for sGC localization and phosphatidylinositol 3,4,5-trisphosphate production but with different refractory periods, by undertaking simultaneous observations of the excitable properties of the two pathways in *Dictyostelium* cells. Owing to the shorter refractory period, sGC signaling responded more frequently to chemoattractants, leading to pseudopod formation with higher frequency. sGC excitability was regulated negatively by its product cGMP and by cGMP-binding protein C (GbpC) through the suppression of F-actin polymerization, providing the underlying delayed negative-feedback mechanism for the cyclical pseudopod formation. These results suggest that parallel pathways respond to environmental cues on different timescales in order to mediate chemotactic motility in a manner based on their intrinsic excitability.

KEY WORDS: cGMP signaling, Chemotaxis, Excitability, Pseudopod formation

INTRODUCTION

Chemotaxis to extracellular chemical signals plays important roles in various physiological phenomena, including neurogenesis, immune response and wound healing (Servant et al., 2000; Kalil and Dent, 2005; Mayor and Etienne-Manneville, 2016). Chemotactic cells, such as mammalian neutrophils and the social amoeba *Dictyostelium discoideum*, detect chemical gradients and migrate directionally by coordinating their anterior pseudopod formation and posterior tail contraction (Van Haastert and Devreotes, 2004; Hind et al., 2016). Evolutionally conserved molecular mechanisms are involved in the bias of cell motility directionally along chemoattractant gradients (Artemenko et al., 2014; Devreotes et al., 2017). In *Dictyostelium* cells, extracellular 3′,5′-cyclic adenosine monophosphate (cAMP) works as a chemoattractant and is detected by G protein-coupled receptors (GPCRs) and cognate heterotrimeric G proteins. This detection activates multiple signaling pathways including those mediated by (1) phosphoinositide 3-kinase, and phosphatase and tensin homolog (PI3K–PTEN), (2) phospholipase A2 (PLA2), (3) TorC2, phosphoinositide-dependent kinase 1 and protein kinase B family proteins (TorC2–PDK–PKB; note the PKB family is also called Akt), and (4) soluble guanylyl cyclase (sGC). Most of these parallel and compensatory pathways generate a polarized signal selectively at the front or back of a motile cell along the cAMP gradient (Cai and Devreotes, 2011; Artemenko et al., 2014; Devreotes et al., 2017). In the PI3K–PTEN pathway, a phosphatidylinositol 3,4,5-trisphosphate (PIP3)-enriched domain localizes to the pseudopod and regulates the polymerization or stabilization of F-actin (Kortholt et al., 2011; Devreotes et al., 2017). Similar localizations of sGC and PKB activities also act as intracellular cues for pseudopod formation (Veltman and Van Haastert, 2006; Kamimura et al., 2008). However, little is known about the relationship between the parallel signaling pathways and their unique functions in chemotaxis.

The spatiotemporal dynamics of PIP3 has been well characterized during the chemotactic motility shown by eukaryotic amoeboid cells such as *Dictyostelium*. A PIP3-enriched domain on the membrane is produced in a self-organized manner independently of cell motility and shows wave-like localization patterns (Asano et al., 2008; Arai et al., 2010; Gerisch et al., 2012). The PIP3-enriched domain spontaneously occurs in the absence of extracellular stimuli, and it has relatively constant biochemical activities and size, of a few microns in diameter. These spontaneous activities are linked to pseudopod formation and are biased along cAMP gradients, leading to a change from random to directional motility (Xiong et al., 2010; Shibata et al., 2013). The PIP3 dynamics has been explained by an intrinsic excitable system. In general, an excitable system shows an all-or-none response to a super-threshold stimulus so that a constant output that is independent of the input strength is assured (Huang et al., 2013; Nishikawa et al., 2014). Thus, the excitable behavior is able to amplify a small input and function as an internal biochemical compass for motile cells (Xiong et al., 2010; Shibata et al., 2013). Human neutrophils also show PIP3 enrichment into membrane domains in a manner consistent with an excitable system, suggesting that this a conserved property of eukaryotic chemotaxis (Tang et al., 2014). Another feature of excitability is characterized by the refractory period, which is the recovery time for the system to react to a second stimulus once its excitation starts. During the refractory state, the system cannot respond even to a stimulus beyond the threshold. Thus, excitability determines the responsiveness of a cell to the environmental stimulus. The PIP3 pathway in *Dictyostelium* cells has a refractory period of ∼60 s (Huang et al., 2013; Nishikawa et al., 2014), which is longer than the time scale at which cells respond to chemical gradients, giving ambiguity to the physiological meaning of the refractory period.

Among parallel pathways, the sGC pathway has been well documented to contribute to the chemotaxis of *Dictyostelium* cells

[1]Laboratory of Single Molecular Biology, Department of Biological Sciences, Graduate School of Science, Osaka University, Toyonaka, Osaka, 560-0043, Japan. [2]Laboratory for Cell Signaling Dynamics, Center for Biosystems Dynamics Research (BDR), RIKEN, Suita, Osaka, 565-0874, Japan. [3]Laboratory of Single Molecule Biology, Graduate School of Frontier Biosciences, Osaka University, Suita, Osaka 565-0871, Japan.

*Authors for correspondence (masahiroueda@fbs.osaka-u.ac.jp; ykamimur@riken.jp)

M.U., 0000-0002-9722-4224

Received 29 December 2017; Accepted 29 October 2018

Journal of Cell Science (2018) 131, jcs214775. doi:10.1242/jcs.214775

(Veltman et al., 2008). A series of mutants in the sGC pathway have been shown to impair chemotaxis to various kinds of chemoattractants, including cAMP and folic acids, demonstrating the importance of the pathway in chemotactic signaling (Kuwayama et al., 1993, 1995). In the sGC pathway, extracellular cAMP induces intracellular cGMP elevation, which serves as a second messenger for tail contraction at the posterior of the cell via the regulation of myosin II (MyoII) (Soll et al., 2009). cGMP is synthesized by two different types of guanylyl cyclase, cytosolic sGC and membrane-embedded guanylyl cyclase A (GCA) (Roelofs et al., 2001; Roelofs and Van Haastert, 2002). sGC mainly contributes to guanylyl cyclase activity during the cell aggregation stage, at ∼5 h after starvation. Bioinformatic analysis has discovered four cGMP-binding candidate proteins, named GbpA–GbpD (Goldberg et al., 2002). All four proteins have cyclic nucleotide-binding motifs, but biochemical experiments have revealed that GbpC is a major cGMP effector (Bosgraaf et al., 2002). The degradation of cGMP is catalyzed by the two cGMP phosphodiesterases GbpA and GbpB (Bosgraaf et al., 2002). By contrast, GbpC serves as the intracellular high-affinity cGMP-binding molecule and is required for MyoII regulation, while GbpD regulates cell adhesion through its guanine nucleotide exchange factor (GEF) activity for Rap1, even though it has no cGMP-binding ability (Bosgraaf et al., 2005; Kortholt et al., 2006). In addition to the regulation of MyoII at the posterior tail, it has been suggested that the sGC pathway has additional function at the pseudopod (Veltman et al., 2005). sGC proteins localize to pseudopods through the N-terminus without the enzymatic domain during random and chemotactic migration, and cAMP stimulation induces transient recruitments of sGC to the membrane in a manner similar to the PIP3 dynamics (Veltman and Van Haastert, 2006). Cells expressing sGC lacking its N-terminus exhibit a high degree of turning, which brings about a loss of cell orientation, an effect that is also seen in *pi3k1*, *pi3k2* double-knockout strains (Bosgraaf and Van Haastert, 2009). These observations suggest that the sGC pathway has characteristics of an excitable system; however, no direct evidence has been obtained experimentally.

Here, we found that sGC and PIP3 show pseudopod localizations at different frequencies in individual cells, and demonstrated that sGC localization shows behavior consistent with it being part of an excitable system including mediating an all-or-none response to cAMP stimulation, and showing a wave-like pattern formation and refractory period. The refractory period of the sGC-mediated signaling pathway was shorter than that of PIP3, and sGC localized to the pseudopod more frequently than PIP3. sGC localization depended on F-actin and was negatively regulated by cGMP and GbpC via F-actin dynamics, indicating that sGC localization and F-actin are incorporated into one excitable network. This regulation explains the short sGC refractory period as well as concomitant pseudopod formation with relatively high frequency. Overall, these results illustrate that multiple signaling pathways regulate pseudopod dynamics differently through their characteristic excitable properties for chemotactic motility.

RESULTS

Multiple signaling pathways have unique dynamics in localization patterns for cell migration

To address how parallel pathways regulate cell migration, we observed the localization patterns of sGC and PIP3 simultaneously in individual cells. Since sGC localizes to pseudopods through its N-terminal region, we used a Halo-tagged sGC protein as a sGC probe (sGC_N–Halo) along with a previously reported PIP3 probe, the GFP-tagged pleckstrin homology domain of *Dictyostelium* PKBA (PH_{PKB}–GFP) (Meili et al., 1999; Veltman and Van Haastert, 2006; Asano et al., 2008). sGC_N–Halo was stained with tetramethylrhodamine (TMR) for multicolor imaging. In wild-type cells co-expressing sGC_N–Halo and PH_{PKB}–GFP, sGC_N signals were observed in all pseudopods, while PIP3 signals were observed in only half of the pseudopods (Fig. 1A; Fig. S1A). Statistical analysis revealed that the localization pattern was classified into three types: pseudopods with sGC_N localization alone (47.8%), pseudopods with sGC_N and PIP3 colocalization (50.2%) and pseudopods with PIP3 alone (2.0%) (n=452 pseudopods from 13 cells) (Fig. 1B). We analyzed several parameters of the pseudopod dynamics, including extended length, life-time, contribution to cell movement and appearance frequency, for each localization pattern by measuring the extended area of the spontaneously formed pseudopods (see Materials and Methods, Fig. S1B). While small extensions were observed in pseudopods with sGC alone, pseudopods with sGC and PIP3 colocalization were coupled with larger extensions (Fig. 1C,D). In fact, the elongation length of pseudopods with sGC and PIP3 colocalization (5.22±2.31 µm, mean±s.d., n=189 pseudopods) was higher than that of sGC alone (3.92±1.79 µm, n=147 pseudopods) (Fig. 1E). To see the sole effect of sGC localization on the pseudopod dynamics, we created *sgcΔ* cells, which express a mutant sGC lacking its N-terminal region (sGCΔN–Halo/*sgcΔ*) but that maintains the catalytic domain needed for cGMP synthesis. PIP3-alone pseudopods in these mutant cells exhibited smaller elongations than pseudopods where sGC and PIP3 were colocalized (4.28±2.16 µm, n=61 pseudopods, versus 5.22±2.31 µm, n=189). Wild-type cells treated with LY294002, a pharmacological PI3K inhibitor, exhibited only small elongations (2.82±1.08 µm, n=39 pseudopods) (Fig. 1E). Consistent with this, the life-time and the contribution to cell motility of pseudopods with both signals were higher than those with sGC alone (Fig. S1C,D). However, the appearance frequency was not significantly different (Fig. S1E). These genetic and pharmacological inhibitions also caused decreases in the velocity of random migration (Fig. S1F). These observations suggest that the two parallel pathways regulate pseudopod formation additively.

We next observed both signaling molecules in cells exposed to a cAMP gradients to see how their pathways regulate pseudopod formation during chemotaxis (Fig. 1F,G; Movie 1). Upon uniform cAMP stimulation, both signaling molecules exhibited a transient localization to the membrane independently of each other (Fig. S1G,H), demonstrating that the two pathways work in parallel. Under cAMP gradients, the localization patterns of both signaling molecules exhibited different characteristic dynamics (Fig. 1F,G; Movie 1). When the source of the chemoattractant gradient was continuously moved around the cell, sGC and PIP3 were able to follow the changes of the position similarly (Fig. 1F; Fig. S1I). By contrast, once the source position was fixed, the membrane localization dynamics of sGC and PIP3 was different (Fig. 1G). The stimulus first induced sGC and PIP3 localization to the same pseudopod, which was followed by a transient disappearance of both signals. Later sGC localization preceded PIP3 localization on the pseudopod, showing that sGC localized to the pseudopod more frequently than PIP3, consistent with the observations in randomly moving cells (Fig. 1A,B). These results demonstrate that both signaling pathways have their own unique dynamics in response to the same cAMP stimulation.

sGC localization follows the all-or-none law

We next determined whether sGC localization has the features of excitability or not. An excitable system shows the same response to any perturbation over a certain threshold because the response is

Journal of Cell Science (2018) 131, jcs214775. doi:10.1242/jcs.214775

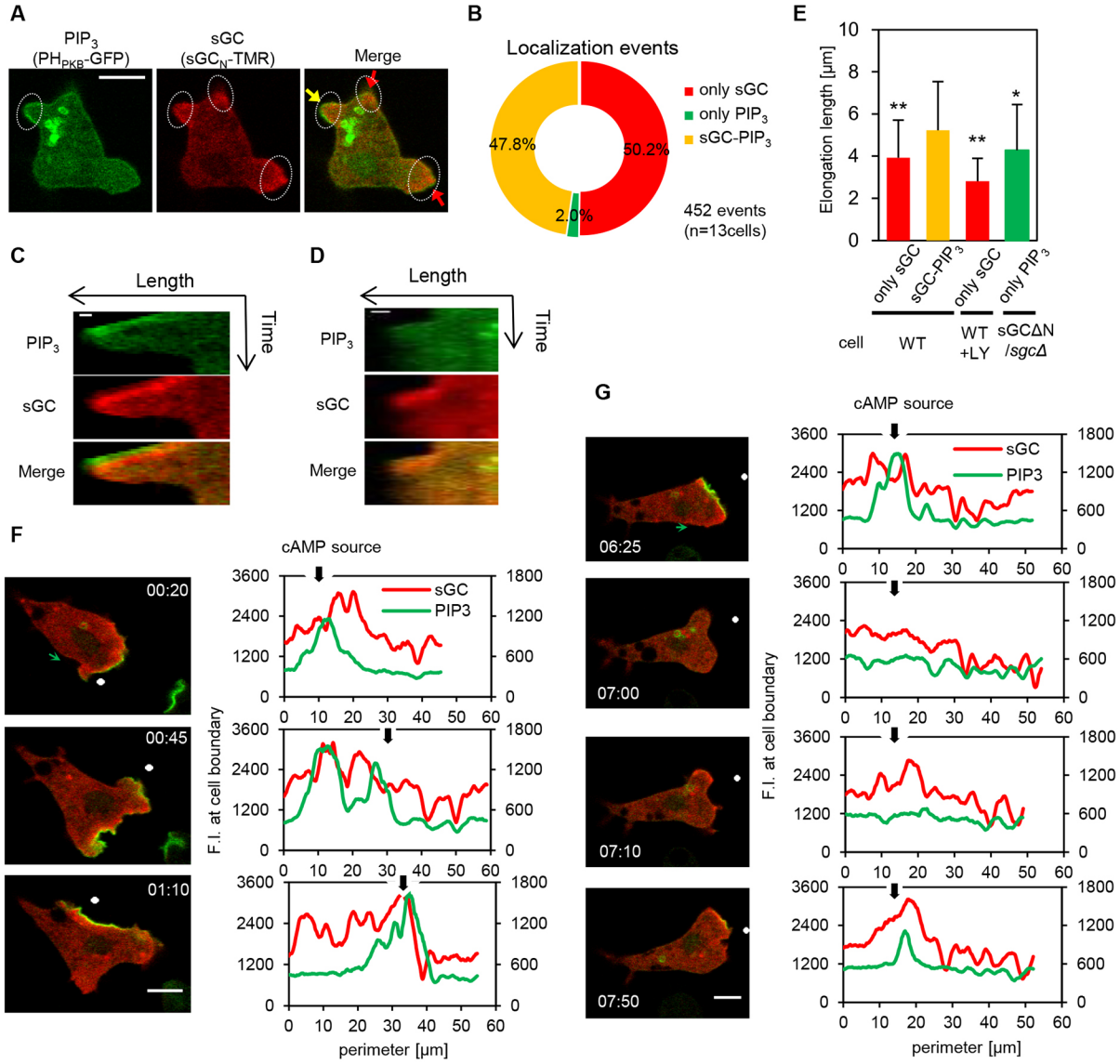

Fig. 1. Simultaneous imaging of sGC and PIP3 localization to the membrane. (A) Representative pseudopods with sGC localization alone (red arrow) or sGC and PIP3 colocalization (yellow arrow) are shown by dotted circles. sGC and PIP3 in a wild-type AX2 cell were visualized by expressing sGC_N–TMR and PH_{PKB}–GFP, respectively. Scale bar: 5 µm. (B) Fraction of pseudopods with sGC, PIP3, or both sGC and PIP3 localization were quantified and are shown in the pie chart. (C,D) The temporal dynamics of sGC_N–TMR and PH_{PKB}–GFP during pseudopod elongation are shown in kymographs (total times shown are 150 s in C and 200 s in D). The bottom surface of a cell was observed by confocal microscopy at 5-s intervals. Pseudopod elongation with localization of sGC_N–TMR and PH_{PKB}–GFP (C) or sGC_N-TMR alone (D) are shown. Scale bars: 1 µm. (E) The elongation length of sGC localized or sGC and PIP3 colocalized pseudopods were measured in wild-type AX2 cells (left). sGC_N-TMR localization in AX2 cells treated with 30 µM LY294002 (middle) and PH_{PKB}–GFP localization in *sgcΔ* expressing sGCΔN–Halo (right) are also shown. Results are mean+s.d. for at least 39 pseudopods. **P*<0.05, ***P*<0.001 versus sGC-PIP3 (Bonferroni test). Spontaneous migration of each cell was recorded for 5–10 min. (F,G) The temporal responsiveness of sGC_N–TMR and PH_{PKB}–GFP to a cAMP gradient. The position of the pipette containing 40 nM cAMP is shown by a white dot in the pictures and black arrows in the profiles. The position of the pipette was moved in F and fixed in G. The fluorescence intensity (F.I.) of sGC and PIP3 along the cell surface was measured starting from the positions of the green arrows in the upper cell images. Time format is mm:ss. Scale bars: 5 µm.

determined by an intrinsic excitable mechanism. Therefore, a pulse cAMP stimulus with a very short duration should trigger the same response in sGC localization to a stepwise cAMP stimulus if the responses are excitable. To determine whether this was the case, we used an experimental system in which caged-cAMP was photolyzed in a flow chamber, allowing us to control the timing and strength of the pulse stimuli by manipulating UV irradiation exposure times (Fig. S2A) (Beta et al., 2007). Upon a UV flash at a region upstream of the cells, the uncaged cAMP is applied to and removed from the cells within a few seconds because of the flow (Fig. S2B), which is short enough to test the excitability of sGC localization (Veltman et al., 2005). A C-terminal fusion of GFP to full-length sGC (sGC–GFP) was expressed in *gcΔ* cells lacking both sGC and GCA, and sGC–GFP localization was observed in response to the transient stimulation. Cytosolic sGC–GFP exhibited translocation to the membrane as a transient response to a pulse stimulus within 2 s of UV exposure as well as upon a step stimulus of 100 nM cAMP (Fig. 2A). The two transient responses had the same temporal changes and same peak amplitude (see Materials and Methods), indicating that the sGC localization dynamics is produced intrinsically by the system itself in a manner that is independent of the stimulus pattern. Furthermore, we examined the dose-dependent

Journal of Cell Science (2018) 131, jcs214775. doi:10.1242/jcs.214775

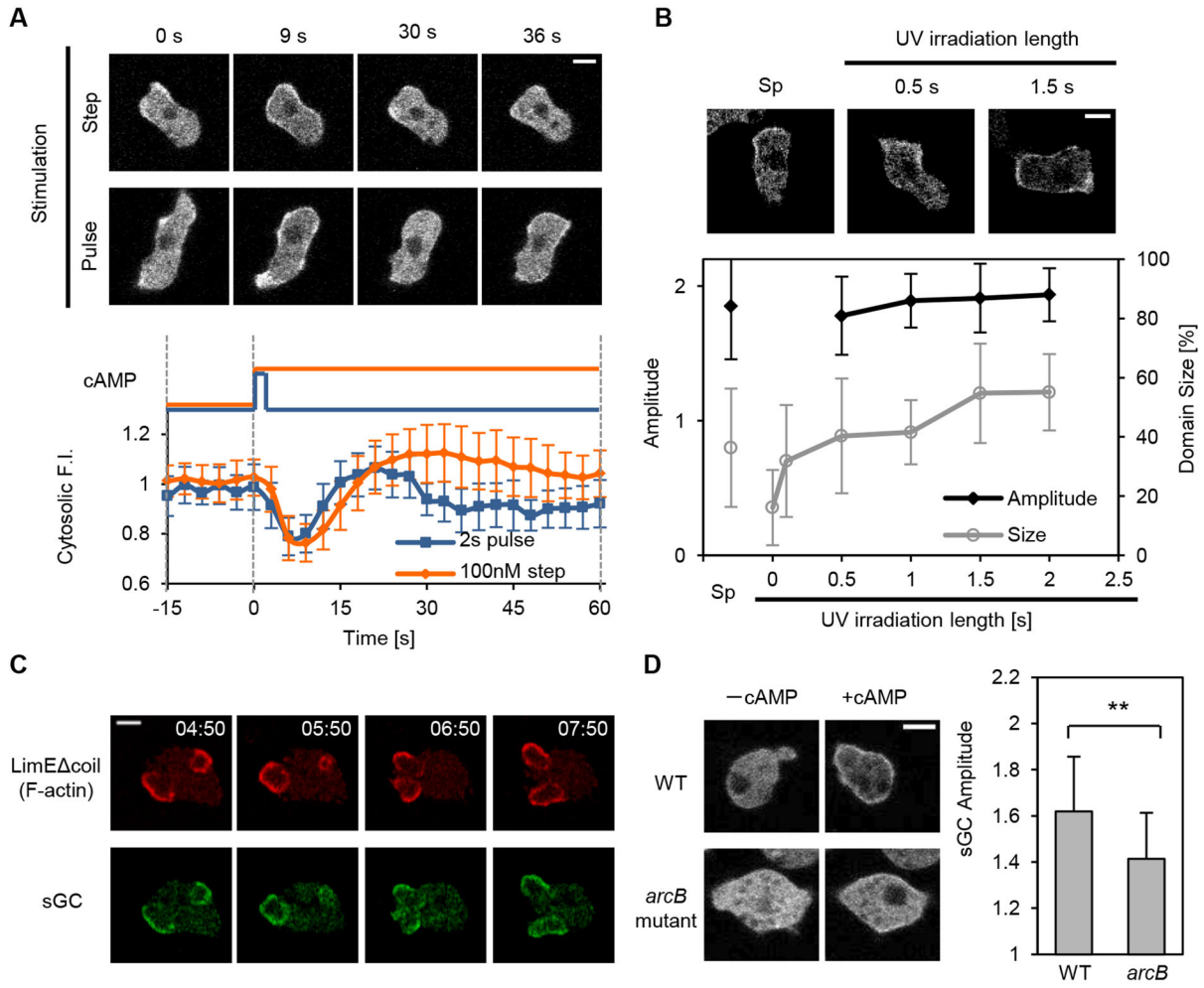

Fig. 2. Excitable dynamics of sGC localization to the membrane. (A) A *gcΔ* cell expressing sGC–GFP was stimulated upon pulse and step inputs of cAMP. Representative images at the indicated times after a 100-nM step (top row) or 2-s pulse (bottom row) stimulus are shown. The bottom panel shows the comparison between sGC–GFP responses to pulse (blue) and step (orange) inputs. Responses (mean±s.d. for *n*=12 and 24 cells, respectively) of cytosolic sGC–GFP [fluorescence intensity (F.I.)] were normalized to the pre-stimulus level. The same data is also shown in Fig. 4A. (B) Excitable features of sGC–GFP localization were assessed by using UV-sensitive caged cAMP (see Materials and Methods). A *gcΔ* cell expressing sGC–GFP was stimulated via various UV exposure times (top). The response amplitude and domain size of the sGC-enriched region are shown as functions of UV exposure time (bottom). Characteristics of the spontaneously formed domain are shown as Sp (mean±s.d. for at least 17 cells). (C) Colocalization pattern of F-actin and sGC. A wild-type AX2 cell co-expressing mRFP–LimEΔcoil and sGC–GFP was treated with 1 µM LatA. The bottom of the cell was observed at 5-s intervals. Time format is mm:ss. (D) Wild-type AX2 and *arcB* mutant cells expressing sGC–GFP were stimulated with 100 nM cAMP. Localization amplitude (mean+s.d. for *n*=24 and 23 cells, respectively) was quantified as in B. ***P*<0.001 (*t*-test). Scale bars: 5 µm.

response of sGC localization to the membrane upon various UV light exposure times. As expected, the cells expanded the domain size of the sGC signals on the membrane with increasing levels of activated cAMP, although the domain amplitudes remained constant (Fig. 2B). To confirm that the uncaging by UV flash provided the expected cAMP concentrations precisely, we uniformly stimulated the cells with the defined cAMP concentrations and observed sGC–GFP translocation to the membrane. Similar to the results in Fig. 2B, the domain size on the membrane increased according to the cAMP concentration until 0.1 nM with constant domain amplitudes (Fig. S2C). These results reflect excitable features, such as stimulus-dependent domain size and constant amplitude, which were observed previously for PIP3 excitation (Nishikawa et al., 2014).

An excitable system often shows wave-like propagation (Sager, 1996; Khamviwath et al., 2013). In *Dictyostelium* cells, PIP3 and F-actin accumulations on the membrane are typical examples of traveling wave generation (Arai et al., 2010; Gerisch et al., 2011). When we mildly perturbed the actin cytoskeleton with a low concentration of latrunculin A, an actin polymerization inhibitor, we found newly polymerized F-actin showed a wave-like propagation on the bottom surface of the cells, as visualized by the fluorescent F-actin probe mRFP–LimEΔcoil (Fig. 2C) (Fischer et al., 2004). The same behavior was observed for sGC–GFP localization, which overlapped the F-actin signals (Fig. 2C; Movie 2). Furthermore, cAMP-elicited sGC localization to the membrane was significantly reduced in mutant cells lacking functional ArcB, a subunit of Arp2/3 complex, which is responsible for actin polymerization (Fig. 2D) (Langridge and Kay, 2007). Overall, these results imply that the excitable behavior of sGC relies on F-actin activity.

sGC shows a unique refractory period that is shorter than that of PIP3

We determined whether sGC localization to the membrane exhibits a refractory period or not. *gcΔ* cells expressing full-length sGC–

Journal of Cell Science (2018) 131, jcs214775. doi:10.1242/jcs.214775

GFP were stimulated repeatedly with pulsed cAMP at different time intervals (Fig. 3A,B). Transient recruitment of sGC–GFP in response to repetitive stimuli at 21-s and 30-s intervals occurred normally. However, in response to repetitive stimuli at 12-s intervals, the first response was normal but the second and third responses were progressively weaker. These results indicate that the sGC localization has a refractory period of between 10 and 20 s. The existence of the all-or-none response, propagating wave and refractory period proves that the sGC signaling pathway is excitable.

Next, we compared the excitable properties of sGC and PIP3 localizations on the membrane. First, we directly evaluated their refractory times by observing cells that co-expressed both sGC_N–Halo and PH_{PKB}–GFP when stimulated repeatedly by means of UV irradiation at 21-s intervals. sGC localization exhibited a response repeatedly to all stimuli, whereas PIP3 did not (Fig. 3C). The refractory period of PIP3 localization was ∼30–60 s (Fig. 3D), consistent with previous reports (Huang et al., 2013; Nishikawa et al., 2014). sGC localized to the membrane in mutant cells lacking *pi3k1*

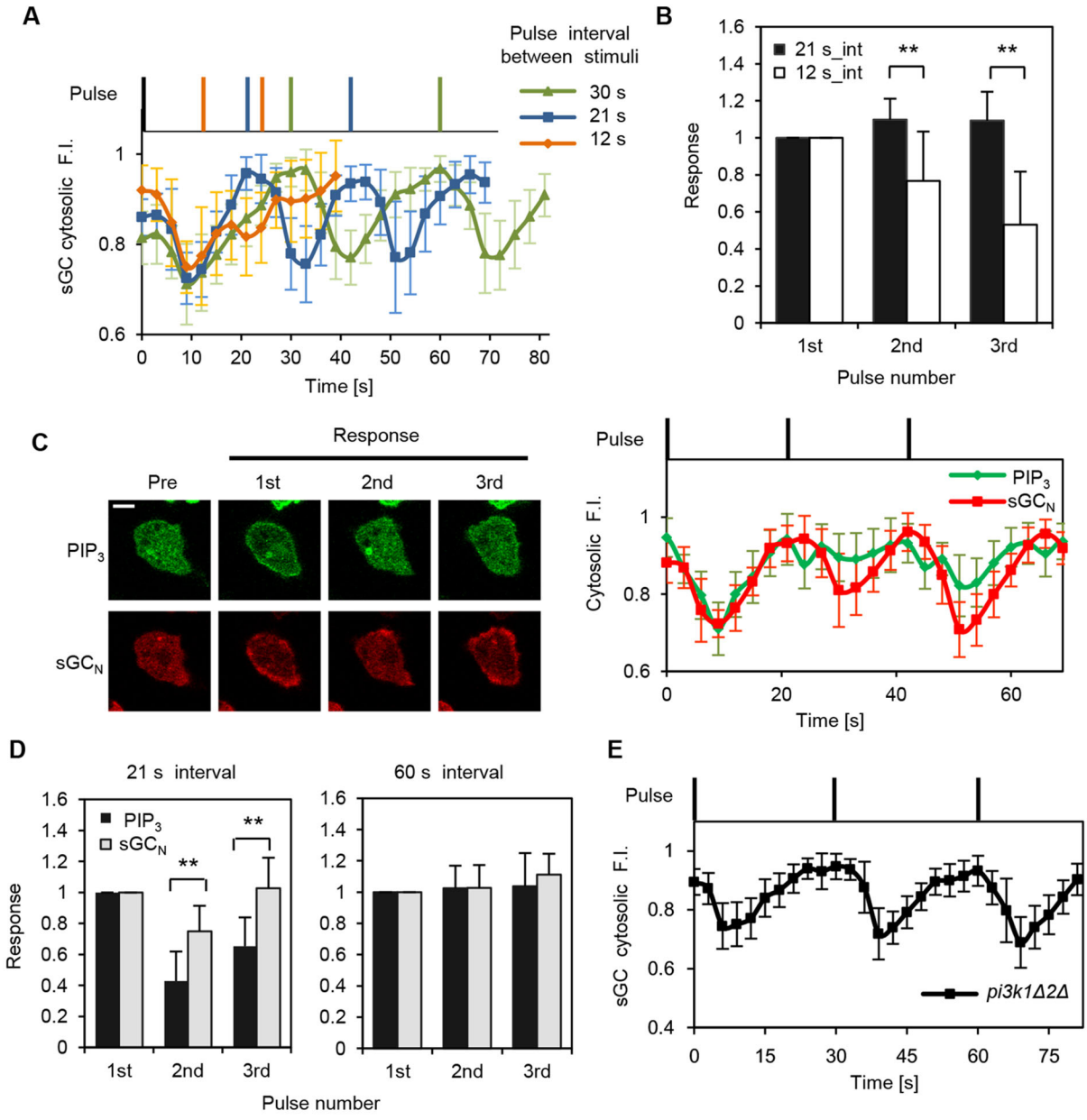

Fig. 3. The sGC-mediated signaling pathway has a shorter refractory period than PIP3-mediated pathway. (A,B) The refractoriness of the sGC-GFP localization to the membrane. (A) A *gcΔ* cell expressing sGC–GFP was stimulated with a 1.5 s of pulsatile UV exposure three times. Cytosolic sGC–GFP responses to stimuli of various interval lengths were normalized to the maximum fluorescence value (F.I.) in the time course. Black and color-coded bars show the first stimulus timing and the pulse timing at different interval lengths, respectively. (B) Each cytosolic response in A was normalized to the value of the first response (mean+s.d. for at least 13 cells). (C,D) A wild-type AX2 cell co-expressing PH_{PKB}–GFP and sGC_N–TMR was stimulated at 21-s (C,D) or 60-s (D) intervals by repetitive pulse stimuli. (C) Cytosolic responses to 21-s interval stimuli were normalized to the maximum fluorescence value in the time course. (D) Refractory responses of PH_{PKB}–GFP and sGC_N–TMR. Each cytosolic response to 21- or 60-s interval stimuli was normalized to the value of the first response (mean+s.d. for n=12 and 10 cells, respectively). (E) sGC–GFP responses to 30-s interval stimuli in *pi3k1Δ2Δ* cells (mean±s.d. for n=16 cells). Black bars at the top in C and E represent the pulse timing. **P<0.001 (t-test). Scale bar: 5 µm.

Journal of Cell Science (2018) 131, jcs214775. doi:10.1242/jcs.214775

and *pi3k2* genes upon repeated stimuli with a refractory period of 30 s, indicating that sGC responsiveness to cAMP stimulation is independent of PIP3 production (Fig. 3E). Thus, the excitable dynamics of sGC has a unique refractory period that is shorter than that of PIP3. Therefore, the sGC pathway can respond to stimulations of short intervals (about 10–20 s), but the PI3K–PTEN pathway cannot.

The cGMP-binding protein GbpC suppresses sGC accumulation on the membrane

To gain molecular insights into the excitable behavior of the sGC pathway, we focused on the possible involvement of both the product of the pathway, cGMP, and its downstream signaling molecules, because excitable systems generally include a delayed negative-feedback mechanism to generate transient excitation (Cao et al., 2016). To reveal the effect of cGMP on sGC localization to the membrane, we first observed mutant sGC with the amino acid change Asp1106Ala, which lacks catalytic activity (sGCΔcat) and was previously expressed as a tagged protein with GFP (sGCΔcat–GFP) in *gcΔ* cells (Veltman and Van Haastert, 2006; Sato et al., 2009). It was reported that *gcΔ* cells expressing sGCΔcat fail to produce cGMP upon cAMP stimulation (Veltman and Van Haastert, 2006). Wild-type sGC–GFP (sGCwt–GFP) exhibited translocation to the membrane transiently upon cAMP stimulation, but the translocation terminated within 20 s. On the other hand, the catalytically dead mutant sGCΔcat–GFP showed prolonged and stronger membrane localization for several minutes (Fig. 4A), indicating that intracellular cGMP accelerates the dissociation of sGC from the membrane. As a control, we examined the response of sGCΔcat–GFP in wild-type cells (Fig. S3A). sGCΔcat–GFP showed translocation to the membrane upon cAMP stimulation in a similar manner to sGCwt–GFP. However, there were some differences in the behavior between sGCwt–GFP and sGCΔcat–GFP after 30 s of stimulation; much more sGCwt-GFP returned to the cytosol than sGCΔcat–GFP, probably because the overproduction of sGCwt–GFP increases the cGMP level in wild-type cells. We also examined the cAMP-mediated responses of wild-type and *gcΔ* cells that expressed a sGC with a deletion of the C-terminal catalytic domain (sGC_N–GFP; Fig. S3B). As expected from the data shown in Fig. 4A, sGC_N–GFP translocated to the membrane within 10 s in both cells, but the returning phase to the cytosol was slower in *gcΔ* cells. In addition, a much higher amount of sGCwt–GFP dissociated from the membrane in wild-type cells than in cells expressing sGC_N-GFP (compare Fig. S3A and S3B). When co-expressed in the same wild-type cells, sGCwt and sGC_N had almost the same dynamics upon cAMP stimulation, reaching equivalent cytosolic levels (Fig. S3C). These results further implicate intracellular cGMP in the dissociation of membrane sGC.

Next, we observed wild-type sGC localization in a series of mutant cells lacking GbpA and GbpB (*gbpABΔ*), GbpC (*gbpCΔ*) or GbpD (*gbpDΔ*). Among them, only *gbpCΔ* cells exhibited defects in sGC–GFP localization, in which sGC–GFP continued to localize on the membrane stably in a manner similar to sGCΔcat–GFP (Fig. 4B). The other mutants exhibited no obvious changes in sGC–GFP localization at resting state without cAMP stimulation (Fig. 4B). When stimulated with cAMP, *gbpCΔ* cells exhibited prolonged sGC–GFP translocation to the membrane, while wild-type cells exhibited transient responses (Fig. 4C). Thus, sGC localization to the membrane is regulated negatively by its product, cGMP, and a cGMP-dependent signaling molecule, GbpC, which ensures the transient response of sGC localization upon cAMP stimulation. In addition, *mhcAΔ* cells, which lack the myosin heavy chain, a gene required for cell contraction at the posterior side (Van Haastert and Devreotes, 2004), exhibited transient sGC localization on the membrane upon cAMP stimulation, although the activity was less efficient than in wild-type cells (Fig. 4C). These results demonstrate that cGMP-dependent GbpC signaling regulates negatively the lifetime of sGC accumulation on the membrane. Because sGC catalyzes cGMP production, this negative regulation by GbpC provides a delayed negative-feedback loop for the sGC excitation pathway.

GbpC regulates the refractory period of the sGC pathway for fast pseudopod cycling

The above results suggest that cGMP-dependent GbpC signaling suppresses sGC localization to the membrane and that this negative feedback regulates recovery to the basal state (i.e. the refractory period) during sGC excitation. In fact, sGC–GFP in *gbpCΔ* cells showed persistent rather than repetitive responses to 12-s and 21-s interval stimuli (Fig. 5A), which resembles the response to step stimuli (Fig. 4C), indicating that cells require GbpC to distinguish repeated pulsatile stimuli from continuous stimuli. Because sGC–GFP in *gbpCΔ* cells responded to repetitive pulse stimuli at 30-s intervals in a manner similar to sGC–GFP in wild-type cells (Figs 3A and 5A), we can conclude that sGC excitation can recover to basal state within 30 s in a GbpC-independent manner. Next, we observed sGC–GFP responses in a *gbpAΔ* cell line, in which the cGMP-specific phosphodiesterase gene is deleted, to see the effects of cGMP on the refractory period, because *gbpAΔ* cells are reported to show prolonged overproduction of cGMP upon cAMP stimulation (Lusche and Malchow, 2005). The *gbpAΔ* cells showed severely suppressed sGC–GFP responses to repeated stimuli at 21-s intervals, while wild-type cells responded normally (Figs 3A and 5B). That is, prolonged cGMP overproduction prolonged the refractory period. Thus, the cGMP-dependent GbpC signaling is required for shortening the refractory period and provides a mechanism for the fast recovery of the sGC pathway in order to respond to the subsequent cAMP stimulation.

To examine the effects of cGMP-dependent GbpC signaling on F-actin polymerization and pseudopod formation in response to cAMP stimulation, we observed mRFP–LimEΔcoil in *gcΔ* and *gbpAΔ* cells, which have defects in the production and degradation of cGMP, respectively (Fig. 5C; Fig. S4A and Movie 3). Wild-type cells showed transient F-actin polymerization at the entire cell surface at ∼10 s after continuous cAMP stimulation, which was followed by the formation of multiple pseudopods with F-actin polymerization for ∼1 min, as observed by mRFP–LimEΔcoil localization. When *gbpAΔ* cells were exposed to the same stimulus, subsequent responses were not observed over the observation period of several minutes, revealing that there was a long suppression of F-actin polymerization. The ectopic expression of GbpA in *gbpAΔ* cells rescued the delay of the secondary response (Fig. 5C, GbpA/*gbpAΔ*).

To further confirm these results, we observed the refractory period in a repetitive stimuli experiment. *gbpAΔ* cells significantly reduced the second response to a 21-s interval stimulus, while wild-type and rescued *gbpAΔ* cells revealed almost the same response to the first and second stimuli (Fig. S4B). On the other hand, both *gcΔ* and *gbpCΔ* cells exhibited enhanced F-actin polymerization (Fig. 5C; Movie 4). This persistent F-actin formation in *gbpCΔ* cells was also observed in a biochemical assay (Fig. 5D; Fig. S4C). GbpC has Ras-like Roc, RasGEF and an mitogen-activated protein kinase kinase kinase (MAPKKK) domain plus a cGMP-binding domain. It has been reported that cGMP binding to GbpC triggers intramolecular signal transduction, ultimately leading to kinase activation (Van Egmond et al., 2008). Therefore, we analyzed the

Journal of Cell Science (2018) 131, jcs214775. doi:10.1242/jcs.214775

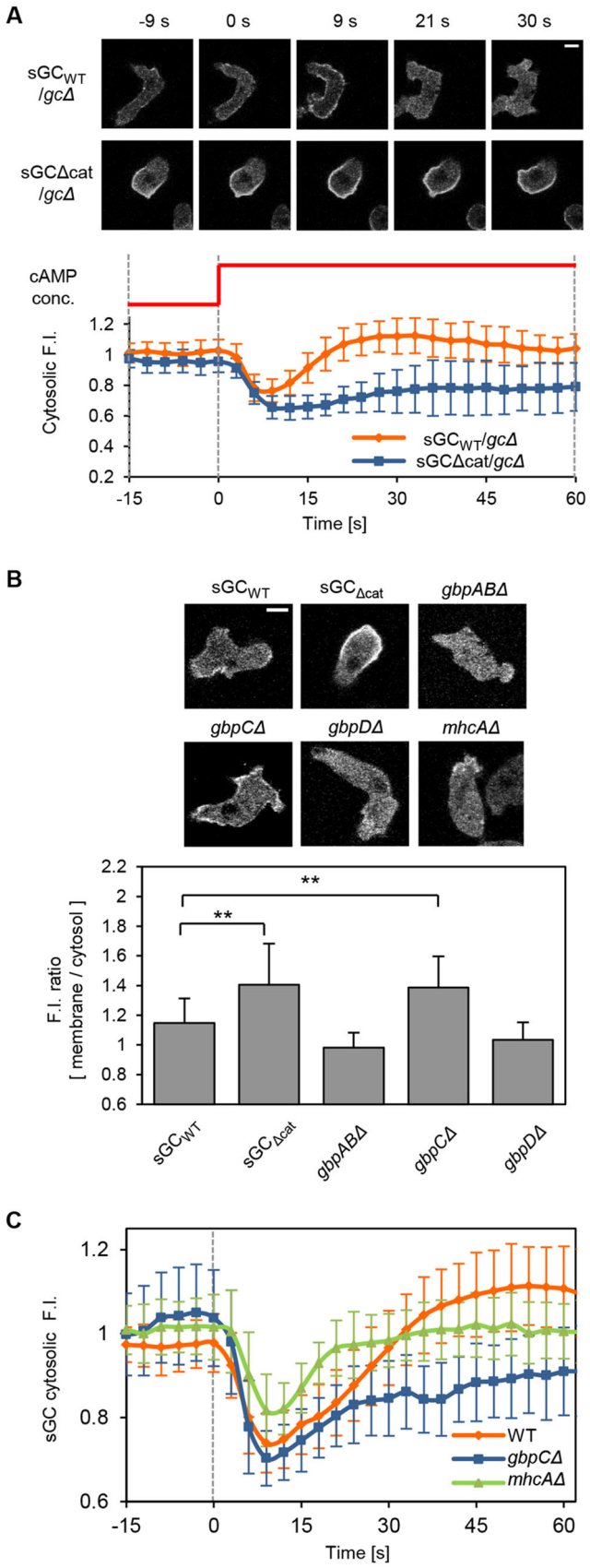

Fig. 4. cGMP-GbpC signaling suppresses sGC localization upon cAMP stimulation. (A) *gcΔ* cells expressing sGC$_{WT}$–GFP or sGC$_{Δcat}$–GFP were stimulated with 100 nM cAMP. Representative images at the indicated times after the cAMP stimulus are shown. The time courses of the cytosolic fluorescence intensity of sGC$_{WT}$ (the same data is shown in Fig. 2A) and sGC$_{Δcat}$ are shown below (mean±s.d. for n=24 and 17 cells, respectively). (B) Pseudopod sGC localization in the indicated knockout cell lines (top). The fluorescence intensity (F.I.) ratio (mean+s.d. for at least 25 cells) between the plasma membrane and the cytosol in the absence of cAMP (bottom). (C) sGC responses of the indicated cell lines upon cAMP stimulation. Wild-type AX3 and mutant cells expressing sGC-GFP were stimulated with 100 nM cAMP. Cytosolic intensity was normalized to the pre-stimulus level (mean±s.d. for at least n=19 cells). **P<0.001 (t-test). Scale bars: 5 µm.

involvement of this intramolecular signaling in GbpC-mediated F-actin regulation using deletion mutants for the MAPKK kinase or the cGMP-binding domains. We found neither mutant was able to rescue the phenotype of excessive F-actin formation upon cAMP stimulation, suggesting that GbpC requires kinase activation following cGMP binding for this regulation (Fig. 5D). These results are consistent with cGMP-dependent GbpC signaling suppressing F-actin polymerization and pseudopod formation. Thus, the negative feedback from cGMP/GbpC to sGC shortens the refractory period of sGC localization to the membrane, which provides a mechanism for high frequency and repetitive pseudopod formation upon cAMP stimulation.

DISCUSSION

Eukaryotic chemotaxis is mediated by parallel signaling pathways that have characteristic features of excitability for the generation of all-or-none signals to regulate pseudopod dynamics at the front of the cells (Cai and Devreotes, 2011; Devreotes et al., 2017). Previous reports have demonstrated the excitable behavior of PIP3 membrane localization during the chemotactic signaling of *Dictyostelium* cells and neutrophil cells (Huang et al., 2013; Nishikawa et al., 2014; Tang et al., 2014). Here, we demonstrated that sGC localization to the membrane was consistent with excitable behaviors, such as an all-or-none response (Fig. 2A,B; Fig. S2C), wave-like pattern formation (Fig. 2C) and refractory period (Fig. 3). These observations indicate the universality of excitable systems in chemotactic signaling pathways. Although both the PI3K–PTEN and sGC pathways have excitable properties, each pathway independently forms an excitable network, as shown by the following findings. First, sGC localization strongly relied on F-actin (Fig. 2D), but F-actin was not essential for PIP3 excitation on the membrane (Arai et al., 2010). Second, sGC responses upon pulse stimuli showed shorter refractory periods (10∼20 s) than PIP3 responses (30∼60 s) (Fig. 3C,D). Finally, the refractory period of sGC localization was independent of PIP3 production (Fig. 3E). These results indicate that each downstream pathway has unique characteristics for their excitable dynamics.

Our observations revealed that sGC localized to the pseudopod more frequently than PIP3 when cells moved along the chemoattractant gradient (Fig. 1F,G). Under constant chemical gradients, it took 10–30 s for sGC to re-localize to the pseudopod once the localization disappeared, which is consistent with the refractory periods seen for sGC responses to pulse stimuli (Fig. 3A). These results suggest that the refractory period for the localization of a signaling molecule corresponds to the frequency of the pseudopod formation. This idea was further supported by observations that showed that modulation of the intracellular cGMP concentration affected the refractory period of sGC responses and pseudopod formation. *gbpAΔ* cells lacking cGMP degradation activity showed prolonged refractory periods (‘refractoriness’), and prolonged suppression of F-actin polymerization and pseudopod formation (Fig. 5B,C; Fig. S4A) (Roelofs et al., 2001; Meima et al., 2002). The

Journal of Cell Science (2018) 131, jcs214775. doi:10.1242/jcs.214775

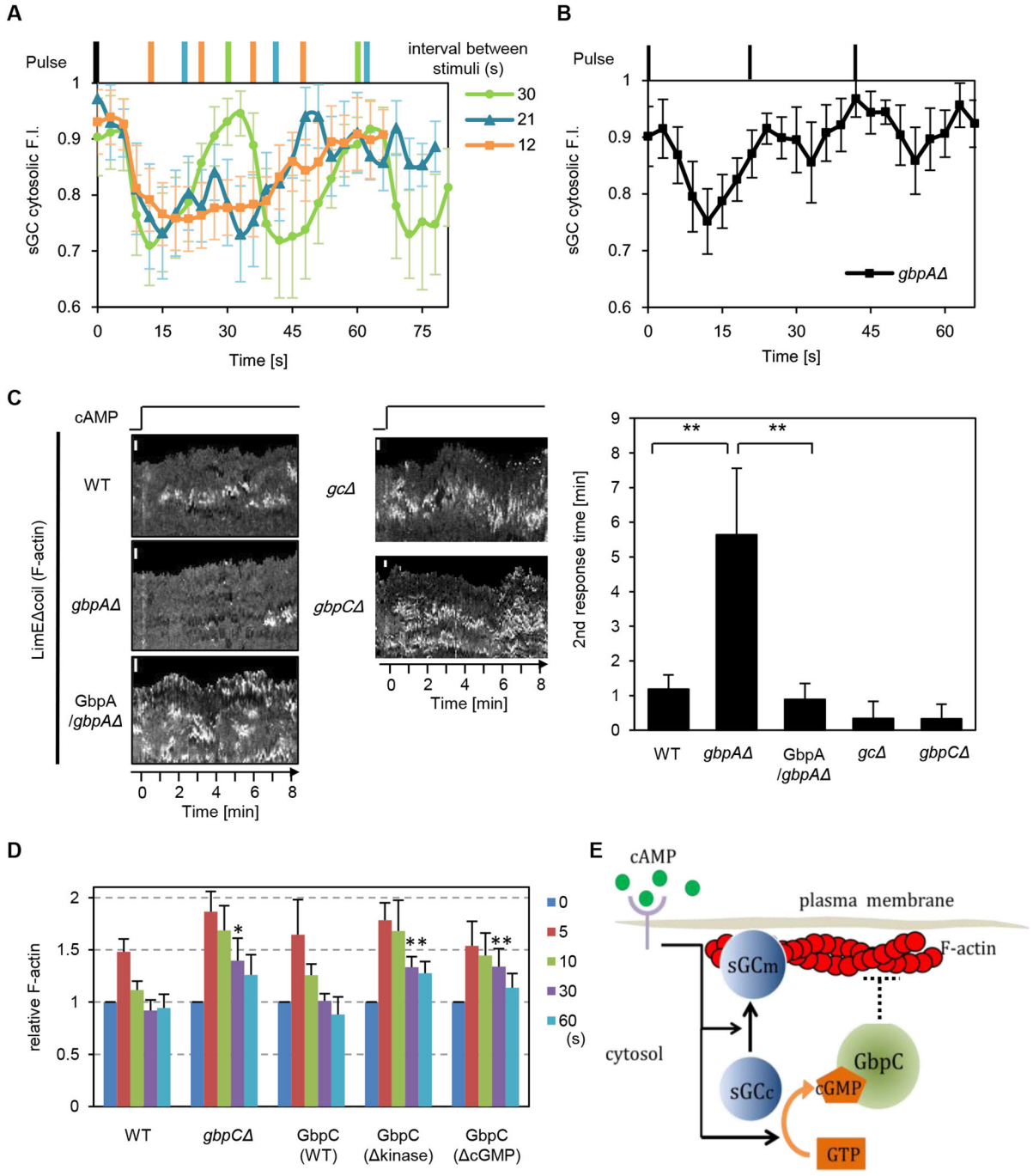

Fig. 5. cGMP–GbpC signaling regulates the refractoriness of sGC responses. (A) Cytosolic sGC–GFP responses in *gbpCΔ* cells upon repetitive stimuli. Color-coded bars represent the pulse timing as shown in Fig. 3 (mean±s.d. for at least 11 cells). (B) The refractoriness of the sGC–GFP response depends on the amount of intracellular cGMP. *gbpAΔ* cells were repetitively stimulated with 21-s interval pulses (mean±s.d. for *n*=16 cells). (C) Temporal dynamics of pseudopod formation upon a cAMP step stimulus. Kymographs of wild-type AX3 and mutant cell lines were drawn by measuring the fluorescence intensity around the boundary of the cell expressing mRFP-LimEΔcoil (left). Scale bars: 5 µm. The second response time represents the time required for secondary pseudopod formation after 10 nM cAMP stimulation at time 0 (right) (mean+s.d. for at least 40 cells). ***P*<0.001 (*t*-test). (D) Cytoskeletal F-actin amounts upon 10 nM cAMP were normalized to the pre-stimulus level. GbpC (WT), GbpC (Δkinase) and GbpC (ΔcGMP) represent *gbpCΔ* cells expressing wild-type, kinase-dead and cGMP-binding mutants of GbpC, respectively (mean+s.d. for at least three experiments). **P*<0.05 versus wild-type, ***P*<0.05 versus GbpC (WT) (*t*-test). (E) A schematic model of the role of the sGC pathway in modulating F-actin dynamics.

prolonged refractoriness has been reported also in *gbpAΔ* cells as a light-scattering response or Ca^{2+} influx upon a cAMP stimulus (Lusche and Malchow, 2005). Furthermore, *gcΔ* and *gbpCΔ* cells showed pseudopod formation more frequently than wild-type cells (Fig. 5C,D; Movie 4).

It has been reported that when stimulated with cAMP twice at 30-s intervals, cells synthesized cGMP upon the first stimulus but not upon the second, indicating some form of adaptation (Van Haastert and Van Der Heijden, 1983). That same report showed that the addition of a cAMP phosphodiesterase enabled cGMP

Journal of Cell Science (2018) 131, jcs214775. doi:10.1242/jcs.214775

production in response to both stimuli. These results suggest that cGMP could be produced repetitively when cAMP stimulation is short enough so as to avoid complete adaptation. Our optical-uncaging experiment was likely to have provided a transient stimulus to the cells before adaptation occurred, although the intracellular cGMP levels were not measured. Based on these observations, we suggest that the refractory period regulated by cGMP-dependent GbpC signaling is a physiologically important feature of chemotactic cell migration.

Although cAMP stimulus induces PIP3 and sGC excitation on the membrane independently (Fig. S1G,H), there may be crosstalk between these pathways. We showed that sGC localization strongly depends on F-actin dynamics (Fig. 2C). Previous studies have shown that F-actin is required for PI3K localization to the pseudopod, and thereby positive feedback comprising Ras, PI3K and F-actin is important for directional cell migration (Sasaki et al., 2004). These observations suggest there is positive feedback between the PI3K–PTEN and sGC pathways that is mediated through F-actin dynamics. This crosstalk could control pseudopod dynamics positively and cooperatively. We further found that pseudopods have different molecular fingerprints, in which most pseudopods showed sGC localization but only half showed both sGC and PIP3 localization (Fig. 1B). Thus, these two types of pseudopods differ. The localization of both sGC and PIP3 leads to more extensive pseudopod extension than the localization of either alone (Fig. 1E). Additionally, the life-times and contribution to cell movement are longer and bigger (Fig. S1C,D). Thus, these parallel pathways regulate the pseudopod elongation additively.

Our results are summarized diagrammatically in Fig. 5E. Chemoattractant stimulations trigger sGC translocation to F-actin on the membrane (Fig. 2C,D). At the same time, sGC catalyzes cGMP production upon chemoattractant stimulation (Roelofs and Van Haastert, 2002). The increased amount of cGMP binds to GbpC directly and induces its kinase activation through a series of intramolecular signals. Then GbpC initiates the destabilization of F-actin and in turn suppresses further pseudopod elongation and induces pseudopod retraction (Fig. 5C). In our model, cGMP-dependent GbpC signaling defines the refractoriness in sGC excitability, which is linked to suppression of the pseudopod. It has been previously reported that GbpC provides major intracellular cGMP-binding sites at a high affinity with a K_d of $\sim 10^{-9}$ M and slow dissociation rate with a halflife of ∼2 min (Van Haastert et al., 1982). These kinetics are not in accordance with our model, which assumes a much faster dissociation for cGMP of 20–30 s. To resolve this discrepancy, an unknown factor with low affinity and fast dissociation to cGMP could function downstream of cGMP-bound GbpC or it is possible that a threshold must be passed for cGMP-bound GbpC to disrupt F-actin stability. Future work will clarify how cGMP regulates F-actin suppression through GbpC.

Previous studies have also shown that cGMP and GbpC signaling activation induces pseudopod suppression at the rear end of cells via the regulation of myosin II (Bosgraaf et al., 2005; Veltman and Van Haastert, 2007). On the other hand, it is known that myosin II is not essential for the retraction of the anterior pseudopod observed in *mhcAΔ* cells (Iwadate and Yumura, 2008). We found myosin II was not essential for sGC excitation upon cAMP stimulation (Fig. 4C). Taken together, our results show that cGMP-dependent GbpC signaling could mediate anterior retraction of the pseudopod, with myosin II making only a minor contribution.

cGMP-dependent GbpC signaling constitutes a delayed negative-feedback in the sGC excitable pathway, which provides a mechanism for the fast cycling of repeated pseudopod formation via shortening of the refractory period. Multiple signaling pathways with different refractory periods can regulate pseudopods at different time scales to mediate chemotaxis. Such pseudopod regulation mechanisms may provide flexibility for motile cells to respond to complex environmental stimulations at various time scales.

MATERIALS AND METHODS

Cell preparation and plasmids

Dictyostelium discoideum cells were grown at 22°C in HL5 medium supplemented with 6 ng/ml vitamin B12 and 100 ng/ml folic acid (Watts and Ashworth, 1970). Wild-type AX2 and AX3 cells were used in this study. The AX2 cell line was used for simultaneous imaging of sGC_N–Halo and PH_{PKB}–GFP, sGC–GFP and mRFP–LimEΔcoil. Because *pi3k1Δ2Δ* and *arcB* mutant cells were derived from the AX2 cell line, sGC–GFP responses in these strains were compared to those in AX2 cells. AX3 cells were used as controls when observing sGC–GFP and mRFP–LimEΔcoil localization, because the mutant strains *gcΔ* (*sgcΔ/gcaΔ*), *gbpAΔ*, *gbpABΔ*, *gbpCΔ*, *gbpDΔ* and *mhcAΔ* were derived from the AX3 cell line. All plasmids and strains are listed in Tables S1 and S2. When grown with selection, medium was supplemented with 10 µg/ml blasticidin S, 20 µg/ml G-418 or 50 µg/ml hygromycin B. Cells were starved for 5–7 h in development buffer consisting of 10 mM Na/KPO_4 pH 6.5, 2 mM $MgSO_4$ and 0.2 mM $CaCl_2$. For cAMP stimulation experiments, cells were treated with 4 mM caffeine for 30 min to inhibit *de novo* adenylyl cyclase activity and deplete extracellular cAMP. Cells were placed on glass-bottom dishes (IWAKI). *sgcΔ* cells were generated from AX2 cells by homologous recombination using a disruption cassette containing the blasticidin S resistance (*BSR*) gene. Two regions of the *sgc* sequence, from 607 to 1116 and 4194 to 4891, were amplified by using the full-length *sgc* gene as a template, and the *BSR* gene was inserted between them. The construct was linearized with *Bam*HI and introduced into AX2 and *sgcΔ* cells, which were selected with 10 µg/ml blasticidin S. The cloned transformants were screened by PCR of their isolated genomic DNAs. The N-terminal fragment of sGC (sGC_N, amino acids 1–1019) and the N-terminal deletion fragment (sGCΔN, amino acids 877–2843) were amplified by PCR and cloned into pHK12-Halo7 to yield C-terminal Halo7-tagged proteins. The full-length *gbpA* gene was amplified by PCR and cloned into pDM358-eGFP to yield C-terminal eGFP-tagged protein.

Fluorescence imaging and pulse cAMP stimulation

Fluorescence images were obtained by using a confocal microscope (FV1000, Olympus) with a 60×/1.35 NA oil-immersion objective lens and software (Fluoview, Olympus). TMR and mRFP were excited by a 543 nm He-Ne laser, and GFP was excited by a 488 nm Ar laser. For pulse cAMP stimulation, cells were placed on a 4-cm round cover glass (Matsunami) with a flow chamber (FCS2, Bioptics). The inlet of the chamber was connected to a 10-ml glass syringe (Top) mounted in the syringe pumps (FP-1000, Melquest). The syringe was filled with development buffer containing 4 mM caffeine and 5 nM DEACM-caged cAMP (Biolog). Photolytic activation of caged cAMP was undertaken with a 405 nm mercury lamp and was carried out upstream of the cells, and activated cAMP was flowed through the system. To demonstrate the temporal change of cAMP concentration, 100 µM CMNB-caged fluorescein (Invitrogen) was used instead of caged cAMP (Fig. S2B). The flow rate was 300 µl/min. In repetitive pulse stimulus experiments, all exposures were carried out via a 1.5-s laser irradiation. To align the first pulse timing, data were normalized by the maximum value of cytosolic fluorescence intensity.

Pseudopod characterization and cell motility assay

Differentiated cells without caffeine treatment were put on a glass-bottom dish and captured by the confocal microscope at 5-s intervals for at least 5 min. The pseudopod dynamics were analyzed by ImageJ according to the localization patterns of sGC and PIP3. The positions of the sGC and PIP3 signals were assigned from the fluorescence images to distinguish two types of localization: sGC alone, and the colocalization of sGC and PIP3.

Morphological changes were extracted by differentiating between two consecutive binarized fluorescence images. In this study, we defined a pseudopod as an area that extended beyond 4 μm^2/frame during growth. These extracted pseudopods were characterized by quantifying their size, appearance frequency, life-time and contribution to cell movement. The size was defined by the elongation length between the beginning and end points of a pseudopod during its total life cycle. The appearance frequency, or the average number of pseudopods per cell, was calculated by dividing the total number of pseudopods on each cell by the recorded time. The life-time is the length of time in which a positive change was maintained in each pseudopod's area. The contribution to cell movement was defined as the displacement of the centroid of a pseudopod during its life-time. For cell motility analysis, differentiated cells without caffeine treatment were observed with an Olympus IX-71 inverted microscope capable of producing phase-contrast optics. Movie files were recorded with a CCD camera (Digital Sight, Nikon) and software (NIS-Elements, Nikon). Cell behavior was recorded for 20 min at 5-s intervals, and images were analyzed using G-Count (G-Angstrom). The motility speed of each cell was calculated as the average speed for each short trajectory.

sGC domain analysis on the cell membrane

Membrane localization of sGC–GFP was analyzed with ImageJ. The fluorescence intensity profile of sGC–GFP on the membrane was obtained at every pixel along the cell periphery and processed with a 15-pixel moving average. In order to compensate for different sGC–GFP expression levels, profiles were normalized to the membrane fluorescence intensity seen in areas without sGC localization. To compare sGC localization under various conditions, we defined localization amplitude and domain size as follows. Localization amplitude represents the maximum value of the normalized intensity along the cell membrane. Domain size was quantified as the ratio of the region with the normalized value exceeding the threshold to the overall membrane area. The threshold was set as 1.2 in this report.

Kymograph analysis

The spatiotemporal dynamics of fluorescence probes on cell membranes was analyzed and shown as 2D patterns with ImageJ. To monitor the pseudopod dynamics of moving cells, kymographs of the mRFP–LimEΔcoil localization in Fig. 5C were generated using an ImageJ plugin. The second response time was defined as the time that a cell showed a new mRFP–LimEΔcoil localization after its first response to 10 nM cAMP. Some cell lines showed a persistent response without transient suppression. The second response time of those cells was defined as 0. sGC_N–TMR and PH_{PKB}–GFP localizations on the bottom surface of the cell in Fig. 1C,D were analyzed via the 'reslice' function in ImageJ after 1.0 pixel mean filtering of movie.

Cytoskeletal actin assay

As previously described (Kamimura et al., 2016), differentiated cells were incubated in phosphate magnesium buffer (2 mM $MgSO_4$ in 5 mM Na/KPO_4 buffer pH 6.5) with 3 mM caffeine at a density of 3×10^7 cells/ml. The cell suspension was stimulated with cAMP at a final concentration of 10 nM. After stimulation, cells were lysed by adding equal volumes of 2× assay buffer consisting of 2% Triton X-100, 20 mM KCl, 20 mM EGTA, 20 mM imidazole and 0.1 mg/ml NaN_3, and incubated on ice for 10 min. The samples were centrifuged at 8000 ***g*** for 4 min to collect the pellet fraction followed by washing with 1× assay buffer and boiled in 2× SDS sample buffer. Finally, the samples were analyzed by PAGE and stained with Coomassie Brilliant Blue. Images were acquired with ImageQuant LAS4000 for the quantification of actin levels (40 kDa).

Acknowledgements

We thank Peter Van Haastert (Dept. Cell Biology, Univ. of Groningen, The Netherlands) for the plasmids expressing sGC–GFP, sGCΔcat–GFP and GbpC mutants, and the National BioResource Project (NBRP)-Nenkin for the AX3, *gbpAΔ*, *gbpABΔ*, *gbpCΔ*, *gbpDΔ*, *mhcAΔ* and *mutated arcB* cells. We appreciate the basic information from DictyBase. We also thank Peter Karagiannis for critically reading the manuscript, and thank all members of the Ueda laboratory for discussions and technical assistance.

Competing interests

The authors declare no competing or financial interests.

Author contributions

Conceptualization: Y.T.; Methodology: Y.T.; Formal analysis: Y.T.; Investigation: Y.T.; Resources: Y.T.; Writing - original draft: Y.T., K.Y., M.U.; Writing - review & editing: Y.T., K.Y., M.U.; Visualization: Y.T.; Supervision: K.Y., M.U.; Project administration: M.U.; Funding acquisition: Y.T., K.Y., M.U.

Funding

This work was supported by Japan Society for the Promotion of Science (JSPS) KAKENHI grant number 15J01805 (to Y.T.), and partially supported by JSPS KAKENHI grant number 17K07396 (to Y.K.), and by the Advanced Research and Development Programs for Medical Innovation (AMED) Core Research for Evolutionary Science and Technology (CREST), grant number JP18gm0910001 (to M.U.).

Supplementary information

Supplementary information available online at
http://jcs.biologists.org/lookup/doi/10.1242/jcs.214775.supplemental

References

Arai, Y., Shibata, T., Matsuoka, S., Sato, M. J., Yanagida, T. and Ueda, M. (2010). Self-organization of the phosphatidylinositol lipids signaling system for random cell migration. *Proc. Natl. Acad.Sci. USA* **107**, 12399-12404.

Artemenko, Y., Lampert, T. J. and Devreotes, P. N. (2014). Moving towards a paradigm: common mechanism of chemotactic signaling in *Dictyostelium* and mammalian leukocytes. *Cell Mol. Life Sci.* **71**, 3711-3747.

Asano, Y., Nagasaki, A. and Uyeda, T. Q. P. (2008). Correlated waves of actin filaments and PIP3 in *Dictyostelium* cells. *Cell Motil. Cytoskeleton* **65**, 923-934.

Beta, C., Wyatt, D., Rappel, W. J. and Bodenschatz, E. (2007). Flow photolysis of spatiotemporal stimulation of single cells. *Anal. Chem.* **79**, 3940-3944.

Bosgraaf, L. and Van Haastert, P. J. M. (2009). Navigation of chemotactic cells by parallel signaling to pseudopod persistence and orientation. *PLoS ONE* **4**, e6842.

Bosgraaf, L., Russcher, H., Smith, J. L., Wessels, D., Soll, D. R. and Van Haastert, P. J. M. (2002). A novel cGMP signaling pathway mediating myosin phosphorylation and chemotaxis in *Dictyostelium*. *EMBO J.* **21**, 4560-4570.

Bosgraaf, L., Waijer, A., Engel, R., Visser, A. J. W. G., Wessels, D., Soll, D. and Van Haastert, P. J. M. (2005). RasGEF-containing proteins GbpC and GbpD have differential effects on cell polarity and chemotaxis in *Dictyostelium*. *J. Cell Sci.* **118**, 1899-1910.

Cai, H. and Devreotes, P. N. (2011). Moving in the right direction: How eukaryotic cells migrate along chemical gradients. *Semin. Cell Dev. Biol.* **22**, 834-841.

Cao, Y., Lopatkin, A. and You, L. (2016). Elements of biological oscillations in time and space. *Nat. Struct. Mol. Biol.* **23**, 1030-1034.

Devreotes, P. N., Bhattacharya, S., Edwards, M., Iglesias, P. A., Lampert, T. and Miao, Y. (2017). Excitable signal transduction networks in directed cell migration. *Annu. Rev. Cell Dev. Biol.* **33**, 103-125.

Fischer, M., Haase, I., Simmeth, E., Gerisch, G. and Müller-Taubenberger, A. (2004). A brilliant monomeric red fluorescent protein to visualize cytoskeleton dynamics in *Dictyostelium*. *FEBS Lett.* **577**, 227-232.

Gerisch, G., Ecke, M., Wischnewski, D. and Schroth-Diez, B. (2011). Different modes of state transitions determine pattern in the phosphatidylinositide-actin system. *BMC Biol.* **12**, 42.

Gerisch, G., Schroth-Diez, B., Müller-Taubenberger, A. and Ecke, M. (2012). PIP3 waves and PTEN dynamics in the emergence of cell polarity. *Biophys. J.* **103**, 1170-1178.

Goldberg, J. M., Bosgraaf, L., Van Haastert, P. J. M. and Smith, J. L. (2002). Identification of four candidate cGMP targets in *Dictyostelium*. *Proc. Natl. Acad. Sci. USA* **99**, 6749-6754.

Hind, L. E., Vincent, W. J. B. and Huttenlocher, A. (2016). Leading from the back: the role of the uropod in neutrophil polarization and migration. *Dev. Cell* **38**, 161-169.

Huang, C. H., Tang, M., Shi, C., Iglesias, P. A. and Devreotes, P. N. (2013). An excitable signal integrator couples to an idling cytoskeletal oscillator to drive cell migration. *Nat. Cell Biol.* **15**, 1307-1316.

Iwadate, Y. and Yumura, S. (2008). Actin-based propulsive forces and myosin-II-based contractile forces in migrating *Dictyostelium* cells. *J. Cell Sci.* **121**, 1314-1324.

Kalil, K. and Dent, E. W. (2005). Touch and go: guidance cues signal to the growth cone cytoskeleton. *Curr. Opin. Neurobiol.* **15**, 521-526.

Kamimura, Y., Xiong, Y., Iglesias, P. A., Hoeller, O., Bolourani, P. and Devreotes, P. N. (2008). PIP_3-independent activation of TorC2 and PKB at the cell's leading edge mediates chemotaxis. *Curr. Biol.* **18**, 1034-1043.

Kamimura, Y., Miyanaga, Y. and Ueda, M. (2016). Heterotrimeric G-protein shuttling via Gip1 extends the dynamic range of eukaryotic chemotaxis. *Proc. Natl. Acad. Sci. USA* **113**, 4356-4361.

Khamviwath, V., Hu, J. and Othmer, H. G. (2013). A continuum model of actin waves in *Dictyostelium discoideum*. *PLoS ONE* **8**, e64272.
Kortholt, A., Rehmann, H., Kae, H., Bosgraaf, L., Keizer-Gunnink, I., Weeks, G., Wittinghofer, A. and Van Haastert, P. J. M. (2006). Characterization of the GbpD-activated Rap1 pathway regulating adhesion and cell polarity in *Dictyostelium discoideum*. *EMBO J.* **281**, 23367-23376.
Kortholt, A., Kataria, R., Keizer-Gunnink, I., Van Egmond, W. N., Khanna, A. and Van Haastert, P. J. M. (2011). *Dictyostelium* chemotaxis: essential Ras activation and accessory signaling pathways for amplification. *EMBO Rep.* **12**, 1273-1279.
Kuwayama, H., Ishida, S. and Van Haastert, P. J. M. (1993). Non-chemotactic *Dictyostelium discoideum* mutants with altered cGMP signal transduction. *J. Cell Biol.* **123**, 1453-1462.
Kuwayama, H., Viel, G. T., Ishida, S. and Van Haastert, P. J. M. (1995). Abberant cGMP-binding activity in non-chemotactic *Dictyostelium discoideum* mutants. *Biochim. Biophys. Acta* **1268**, 214-220.
Langridge, P. D. and Kay, R. R. (2007). Mutants in the *Dictyostelium* Arp2/3 complex and chemoattractant-induced actin polymerization. *Exp. Cell Res.* **313**, 2563-2574.
Lusche, D. F. and Malchow, D. (2005). Developmental control of cAMP-induced Ca2+-influx by cGMP: influx is delayed and reduced in a cGMP-phosphodiesterase D deficient mutant of *Dictyostelium discoideum. Cell Calcium* **37**, 57-67.
Mayor, R. and Etienne-Manneville, S. (2016). The front and rear of collective cell migration. *Nat. Rev. Mol. Cell Biol.* **17**, 98-109.
Meili, R., Ellsworth, C., Lee, S., Reddy, T. B. K., Ma, H. and Firtel, R. A. (1999). Chemoattractant-mediated transient activation and membrane localization of Akt/PKB is required for efficient chemotaxis to cAMP in *Dictyostelium*. *EMBO J.* **18**, 2092-2105.
Meima, M. E., Biondi, R. M. and Schaap, P. (2002). Identification of a novel type of cGMP phosphodiesterase that is defective in the chemotactic *stmF* mutants. *Mol. Biol. Cell* **13**, 3870-3877.
Nishikawa, M., Hörning, M., Ueda, M. and Shibata, T. (2014). Excitable signal transduction induces both spontaneous and directional cell asymmetries in the phosphatidylinositol lipid signaling system for eukaryotic chemotaxis. *Biophys. J.* **106**, 723-734.
Roelofs, J. and Van Haastert, P. J. M. (2002). Characterization of two unusual guanylyl cyclases from *Dictyostelium*. *J. Biol. Chem.* **277**, 9167-9174.
Roelofs, J., Meima, M., Schaap, P. and Van Haastert, P. J. M. (2001). The *Dictyostelium* homologue of mammalian soluble adenylyl cyclase encodes a guanylyl cyclase. *EMBO. J.* **20**, 4341-4348.
Sager, B. M. (1996). Propagation of traveling waves in excitable media. *Genes Dev.* **10**, 2237-2250.
Sasaki, A. T., Chun, C., Takeda, K. and Firtel, R. A. (2004). Localized Ras signaling at the leading edge regulates PI3K, cell polarity, and directional cell movement. *J. Cell Biol.* **167**, 505-518.
Sato, M. J., Kuwayama, H., van Egmond, W. N., Takayama, A. L. K., Takagi, H., van Haastert, P. J. M., Yanagida, T. and Ueda, M. (2009). Switching direction in electric-signal-induced cell migration by cyclic guanosine monophosphate and phosphatidylinositol signaling. *Proc. Natl. Acad. Sci. USA* **106**, 6667-6672.
Servant, G., Weiner, O. D., Herzmark, P., Balla, T., Sedat, J. W. and Bourne, H. R. (2000). Polarization of chemoattractant receptor signaling during neutrophil chemotaxis. *Science* **287**, 1037-1040.
Shibata, T., Nishikawa, M., Matsuoka, S. and Ueda, M. (2013). Intracellular encoding of spatiotemporal guidance cues in a self-organizing signaling system for chemotaxis in *Dictyostelium* cells. *Biophys. J.* **105**, 2199-2209.
Soll, D. R., Wessels, D., Kuhl, S. and Lusche, D. F. (2009). How a cell crawls and the role of cortical myosin II. Eukaryot. *Cell* **8**, 1381-1396.
Tang, M., Wang, M., Shi, C., Iglesias, P. A., Devreotes, P. N. and Huang, C. H. (2014). Evolutionarily conserved coupling of adaptive and excitable networks mediates eukaryotic chemotaxis. *Nat. Commun.* **5**, 5175.
Van Egmond, W. N., Kortholt, A., Plak, K., Bosgraaf, L., Bosgraaf, S., Keizer-Gunnink, I. and. Van Haastert, P. J. M. (2008). Intramolecular activation mechanism of the *Dictyostelium* LRRK2 homolog Roco protein GbpC. *J. Biol. Chem.* **283**, 30412-30420.
Van Haastert, P. J. M. and Devreotes, P. N. (2004). Chemotaxis: signaling the way forward. *Nat. Rev. Mol. Biol. Cell* **5**, 626-634.
Van Haastert, P. J. M., Van Walsum, H. and Pasveer, F. J. (1982). Nonequilibrium kinetics of a cyclic GMP-binding protein in *Dictyostelium discoideum*. *J. Cell Biol.* **94**, 271-278.
Van Haastert, P. J. M. and Van Der Heijden, P. R. (1983). Excitation, adaptation, and deadaptation of the cAMP-mediated cGMP response in *Dictyostelium discoideum*. *J. Cell Biol.* **96**, 347-353.
Veltman, D. M. and Van Haastert, P. J. M. (2006). Guanylyl cyclase protein and cGMP product independently control front and back of chemotaxing *Dictyostelium* cells. *Mol. Biol. Cell* **17**, 3921-3929.
Veltman, D. M. and Van Haastert, P. J. M. (2007). The role of cGMP and the rear of the cell in *Dictyostelium* chemotaxis and cell streaming. *J. Cell Sci.* **121**, 120-127.
Veltman, D. M., Roelofs, J., Engel, R., Visser, A. J. and Van Haastert, P. J. M. (2005). Activation of soluble guanylyl cyclase at the leading edge during *Dictyostelium* chemotaxis. *Mol. Biol. Cell* **16**, 976-983.
Veltman, D. M., Keizer-Gunnik, I. and Van Haastert, P. J. M. (2008). Four key signaling pathways mediating chemotaxis in Dictyostelium discoideum. *J. Cell Biol.* **180**, 747-753.
Watts, D. J. and Ashworth, J. M. (1970). Growth of myxamoebae of the cellular slime mould *Dictyostelium discoideum* in axenic culture. *Biochem. J.* **119**, 171-174.
Xiong, Y., Huang, C. H., Iglesias, P. A. and Devreotes, P. N. (2010). Cells navigate with a local-excitation, global-inhibition-biased excitable network. *Proc. Natl Acad. Sci. USA* **107**, 17079-17086.

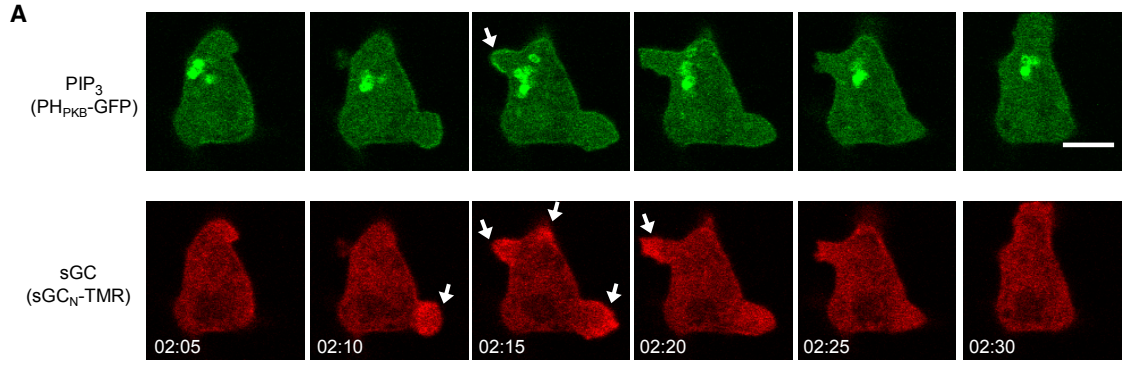

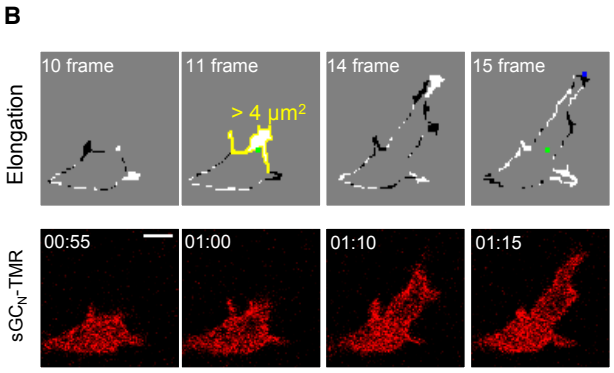

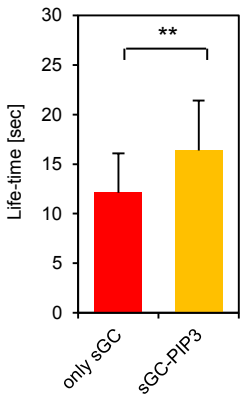

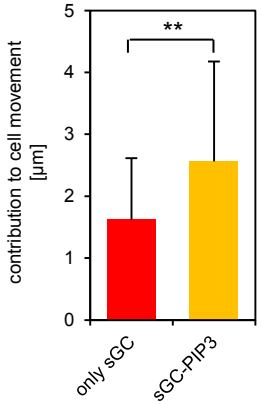

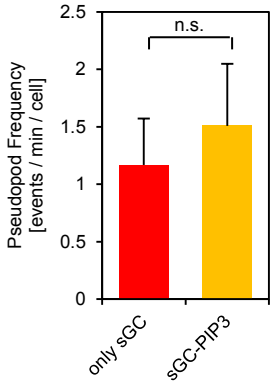

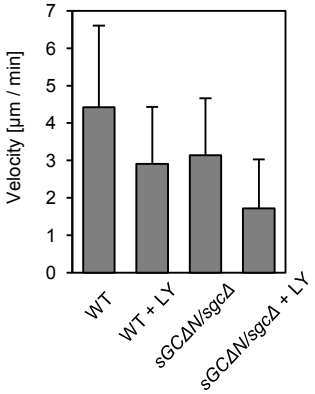

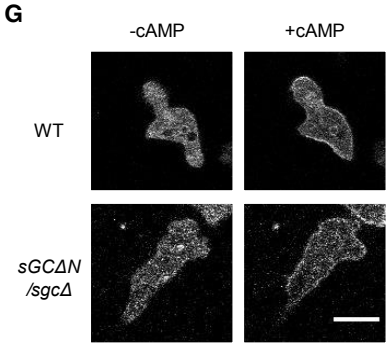

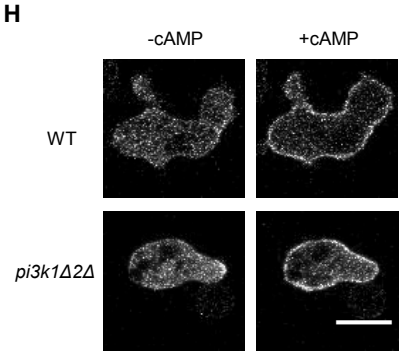

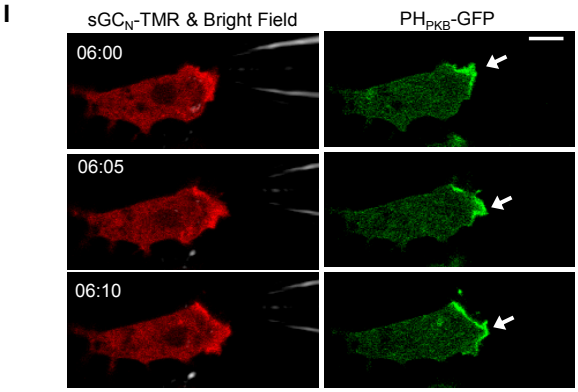

Fig. S1. Independent function of parallel pathways
(A) The time evolution of pseudopod dynamics shown in Figure 1A. sGC and PIP3 localizations are indicated by white arrows. (B) A representative pseudopod analysis. The fluorescence image of a cell with sGC_N-TMR, shown in the bottom, was binarized and subtracted in two consecutive frames. The white and black colors in the upper panel show the positive and negative changes, respectively. An area more than 4 μm^2 (shown by the yellow ROI) was defined as a pseudopod and was pursued when it stopped expanding. The green and blue dots show the start and end points of the pseudopod, respectively. (C) The life-time of pseudopods with sGC alone or with the co-localization of sGC and PIP3 (mean + s.d. for n = 147 and 189 pseudopods, respectively). (D) Contribution to cell movement for pseudopods with sGC alone or with the co-localization of sGC and PIP3 (mean + s.d. for n = 147 and 189 pseudopods, respectively). (E) Frequencies of pseudopod formation with sGC alone or with the co-localization of sGC and PIP3. The number of pseudopods was counted if the elongation area was over 4 μm^2 (mean + s.d. for n = 13 cells). (F) Migration velocity of wild-type AX2 and *sgcΔ* cells expressing sGCΔN-Halo was analyzed in the presence or absence of 50 μM LY294002 (see Methods). (G and H) PIP3 and sGC responses of the indicated cell lines at 1 μM cAMP. PIP3 production of wild-type AX2 and sGCΔN / *sgcΔ* cells (G) and sGC localization of wild-type AX2 and *pi3k1Δ2Δ* cells (H) were observed by the expression of PH_{PKB}-GFP and sGC-GFP, respectively. (I) Image galleries of a cell with sGC (red) and PIP3 (green) signals taken from supplementary Movie 1. The elongating pseudopod is shown by white arrows. Time format is “mm:ss”. Scale bars are 5 and 10 μm in (A)-(C) and (H)-(I), respectively (** $P < 0.01$, t-test).

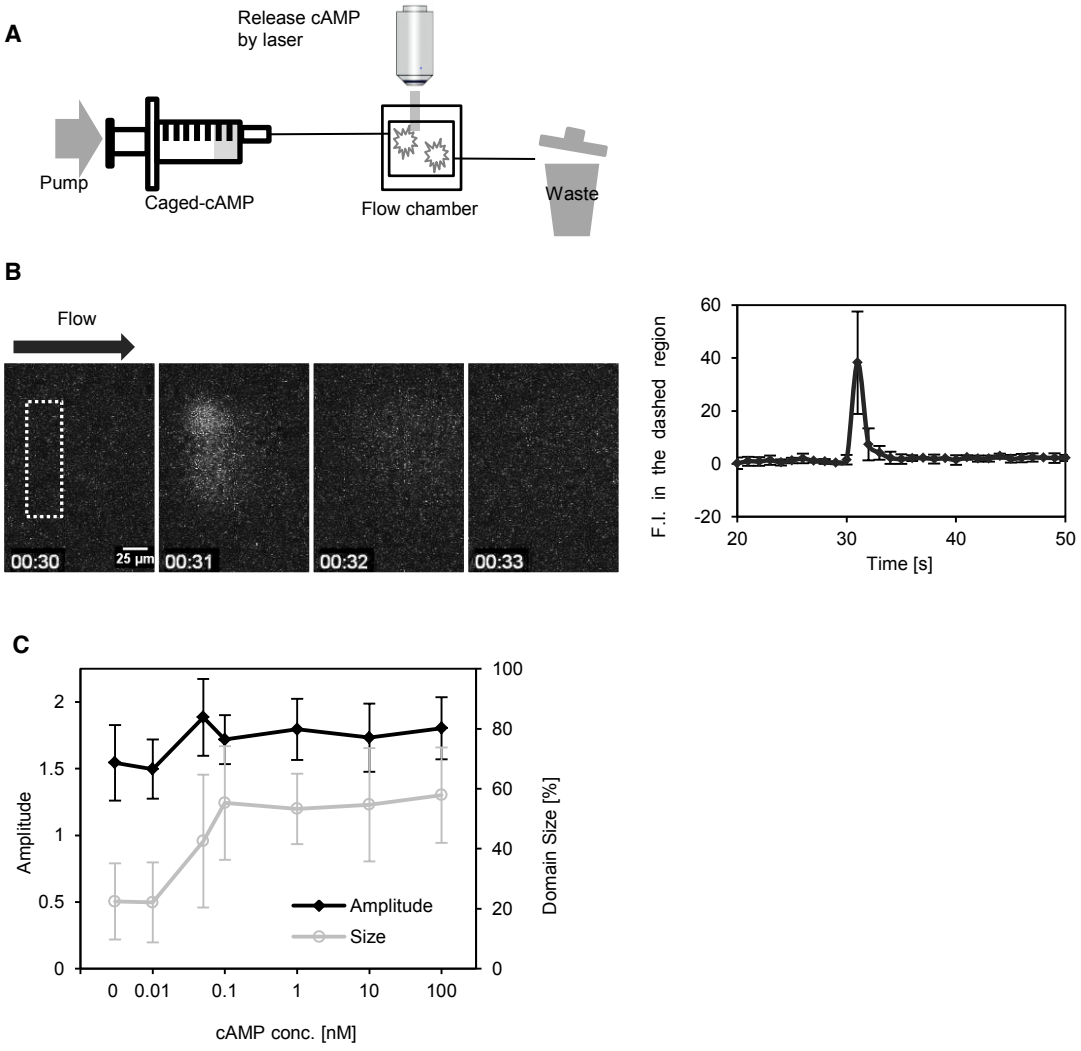

Fig. S2. Construction of the cAMP pulse stimulation system

(A) A schematic drawing of the pulse stimulation system. (B) Time course of the transient release of caged compound. Photolysis of 100 µM caged fluorescein in solution was carried out at the dashed region by UV flash (left). Fluorescence intensity of the region where UV was irradiated (right) (mean ± s.d. for n = 3). (C) *gcΔ* cells expressing sGC-GFP were stimulated with various cAMP concentrations. Response amplitude and domain size of the sGC-enriched region are shown as functions of cAMP concentrations. (mean ± s.d. for at least 8 cells).

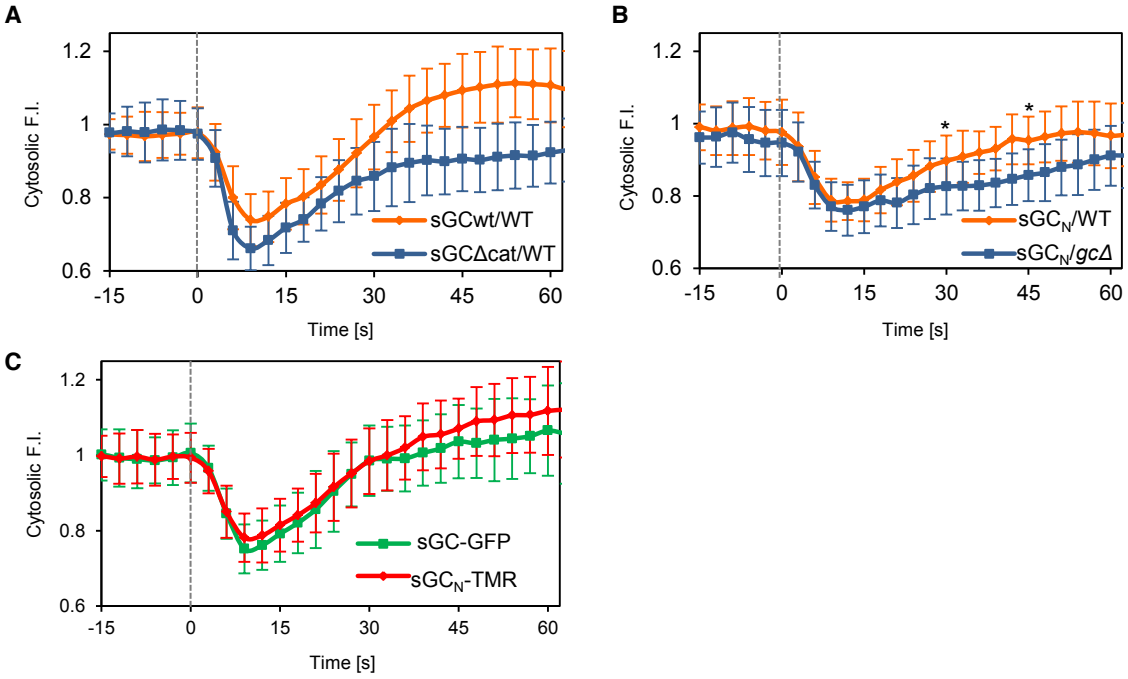

Fig. S3. Evaluation of various sGC constructs

(A) sGC responses of the indicated cell lines upon cAMP stimulation. Wild-type AX3 cells expressing sGC$_{WT}$-GFP or sGC$_{\Delta cat}$-GFP were stimulated with 100 nM cAMP. Cytosolic intensity was normalized to the pre-stimulus level (mean ± s.d. for at least n = 19 cells). For sGC$_{WT}$-GFP, the same data is shown in Figure 4C. (B) The responses of the N terminus of sGC (sGC$_N$) in wild-type or *gcΔ* cells were observed as in (A) (mean ± s.d. for n = 29 and 28 cells, respectively; * $P < 0.01$ versus wild-type cell at 30 and 45 sec, t-test). (C) The responses of the full-length (sGC) and the N-terminal sGC (sGC$_N$) in the same wild-type cell were observed as in (A) (mean ± s.d. for n = 19 cells).

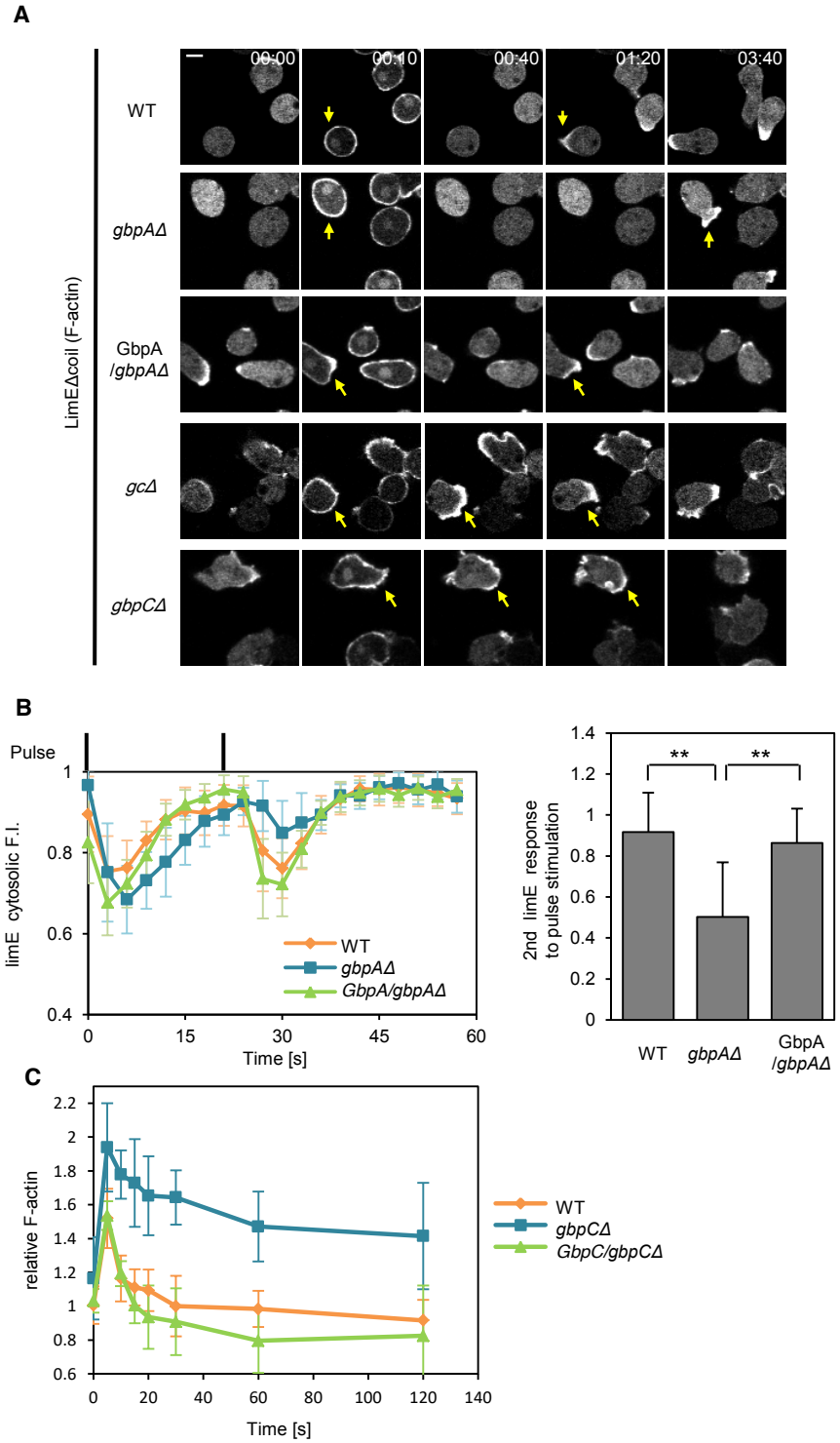

Fig. S4. The recovery time of F-actin response depends on cGMP concentration
(A) Wild-type AX3 and mutant cell lines expressing mRFP-LimEΔcoil were stimulated with 10 nM cAMP. Yellow arrows show the pseudopods where mRFP-LimEΔcoil localized. These pictures were clipped from Movies 3 and 4. (B) The refractoriness of F-actin depends on the amount of intracellular cGMP. Wild-type AX3, *gbpAΔ* and *gbpAΔ* rescued by GbpA cells expressing mRFP-LimEΔcoil were repetitively stimulated with 21-sec interval pulses (left) (mean ± s.d. for n = 23 cells). Cytosolic responses to 21-sec interval stimuli were normalized by the maximum fluorescence value in the time course. Black bars on the abscissa represent the pulse timing. The second responses normalized by the first responses of each cell line are shown (right) (mean + s.d.; ** $P < 0.001$, t-test). (C) Cytoskeletal F-actin amounts upon 10 nM cAMP shown in Figure 5D were normalized to the value of wild-type cells at 0 sec (mean ± s.d. for at least 3 experiments).

Table S1. Plasmid list.

Plasmid name	Protein expressed	Tag	Backbone	Source or reference
sGC-GFP	SgcA	GFP	pMB74	Veltman et al., 2005
sGCΔcat-GFP	SgcA(D1106A)	GFP	pMB74	Veltman et al., 2006
sGCN-Halo7	SgcA(1-1019)	Halo7	pHK12	this study
sGCΔN-Halo7	SgcA(877-2843)	Halo7	pHK12	this study
PH_{PKB}-eGFP	PkbA(1-113)	eGFP	pBIG	Meili et al., 1999
mRFP-LimEΔcoil	LimE(1-145)	mRFP	pHK12	this study
GbpA-eGFP	GbpA	eGFP	pDM358	this study

Numbers in parentheses refer to a mutation or regions of amino acid residues.

Table S2. Strain list.

Strain name	Genotype	Background	Source or reference
AX2		AX2	Lab stock
AX3		AX3	NBRP
sgcΔ	*sgcAΔ*	AX2	this study
gcΔ	*sgcAΔ, gcAΔ*	AX3	Veltman et al., 2006
pi3k1Δ/pi3k2Δ	*pikAΔ, pikBΔ*	AX2	Kamimura et al., 2016
gbpAΔ	*pdeDΔ*	AX3	Bosgraaf et al., 2002
gbpABΔ	*pdeDΔ, pdeEΔ*	AX3	Bosgraaf et al., 2002
gbpCΔ	*gbpCΔ*	AX3	Bosgraaf et al., 2002
gbpDΔ	*gbpDΔ*	AX3	Bosgraaf et al., 2002
mhcAΔ	*mhcAΔ*	AX3	Ruppel et al., 1994
arcB	arcB(I191L/D197Y/K206V/A213V/F223L/P224S/E232G/I237T/H245L/S250S)	AX2	Langridge and Kay, 2007
PH_{PKB}-eGFP, sGC_N-Halo7/AX2		AX2	this study
sGC-GFP/mRFP-LimEΔcoil /AX2		AX2	this study
sGC-GFP/AX2		AX2	this study
mRFP-LimEΔcoil/AX3		AX3	this study
sGCΔN-Halo7/*sgcΔ*	*sgcAΔ*	*sgcΔ*	this study
PH_{PKB}-eGFP, sGCΔN-Halo7 /*sgcΔ*	*sgcAΔ*	*sgcΔ*	this study
sGC-GFP/*gcΔ*	*sgcAΔ, gcAΔ*	*gcΔ*	Sato et al., 2009

NBRP, National BioResource Project in Japan.

Strain name	Genotype	Background	Source or reference
sGCΔcat-GFP/*gc Δ*	*sgcAΔ, gcAΔ*	*gcΔ*	Sato et al., 2009
mRFP-LimEΔcoil/*gcΔ*	*sgcAΔ, gcAΔ*	*gcΔ*	this study
sGC-GFP/*pi3k1Δ2Δ*	*pikAΔ, pikBΔ*	*pi3k1Δ /pi3k2Δ*	this study
sGC-GFP/*gbpAΔ*	*pdeDΔ*	*gbpAΔ*	this study
mRFP-LimEΔcoil/*gbpAΔ*	*pdeDΔ*	*gbpAΔ*	this study
mRFP-LimEΔcoil/GbpA-eGFP /*gbpAΔ*	*pdeDΔ*	*gbpAΔ*	this study
sGC-GFP/*gbpABΔ*	*pdeDΔ, pdeEΔ*	*gbpABΔ*	this study
sGC-GFP/*gbpCΔ*	*gbpCΔ*	*gbpCΔ*	this study
GbpC/*gbpCΔ*	*gbpCΔ*	*gbpCΔ*	van Egmond et al., 2008
GbpCΔcGMP/*gbpCΔ*	*gbpCΔ*	*gbpCΔ*	van Egmond et al., 2008
GbpCΔkinase/*gbpCΔ*	*gbpCΔ*	*gbpCΔ*	van Egmond et al., 2008
mRFP-LimEΔcoil/*gbpCΔ*	*gbpCΔ*	*gbpCΔ*	this study
sGC-GFP/*gbpDΔ*	*gbpDΔ*	*gbpDΔ*	this study
sGC-GFP/*mhcAΔ*	*mhcAΔ*	*mhcAΔ*	this study
sGC-GFP/*arcB*	arcB(I191L/D197Y/K206V/A213V/F223L/P224S/E232G/I237T/H245L/S250S)	*arcB*	this study

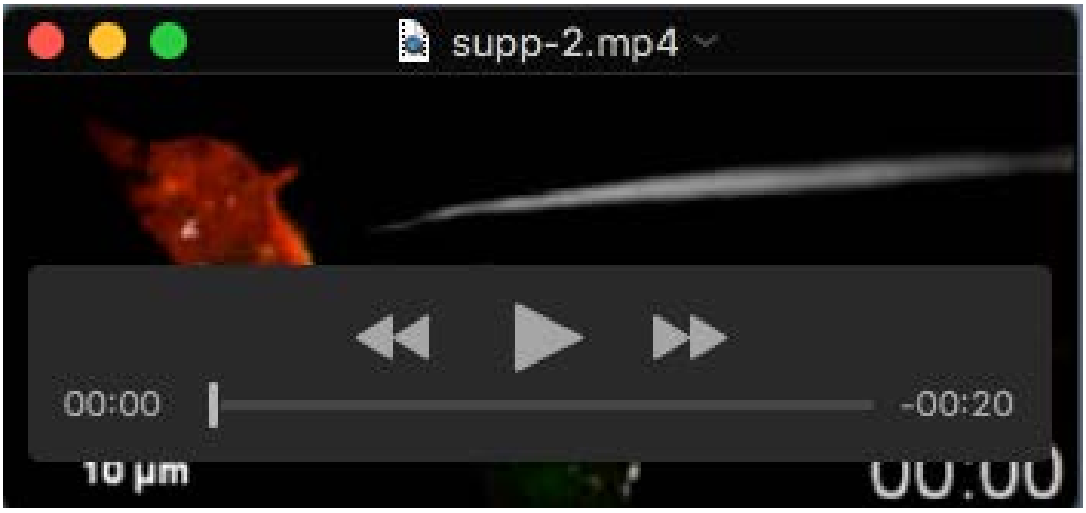

Movie 1. Chemotactic sGC and PIP3 responses under a cAMP gradient.

Wild-type AX2 cells expressing PH_{PKB}-GFP (green) and sGC_N-TMR (red) were stimulated with a pipette containing 40 nM cAMP. The position of the pipette (grey) was controlled by hand manipulation. The video was captured every 5 sec and is shown at 10 frame/sec. Time format is "mm:ss".

Movie 2. Wavelike pattern of sGC and F-actin localization.

A wild-type AX2 cell expressing sGC-GFP and mRFP-LimEΔcoil was pretreated with 1 µM LatA for 30 min. The bottom layer of the cell was observed by confocal microscopy at 5-sec intervals. Time format is "mm:ss".

Movie 3. F-actin responses to 10 nM cAMP, related to Fig. 5.

mRFP-LimEΔcoil was observed in wild-type AX3, *gbpAΔ*, and GbpA-eGFP-expressing *gbpAΔ* cells. cAMP was added at 30 sec. The video was captured every 5 sec and is shown at 12 frame/sec. Time format is "mm:ss".

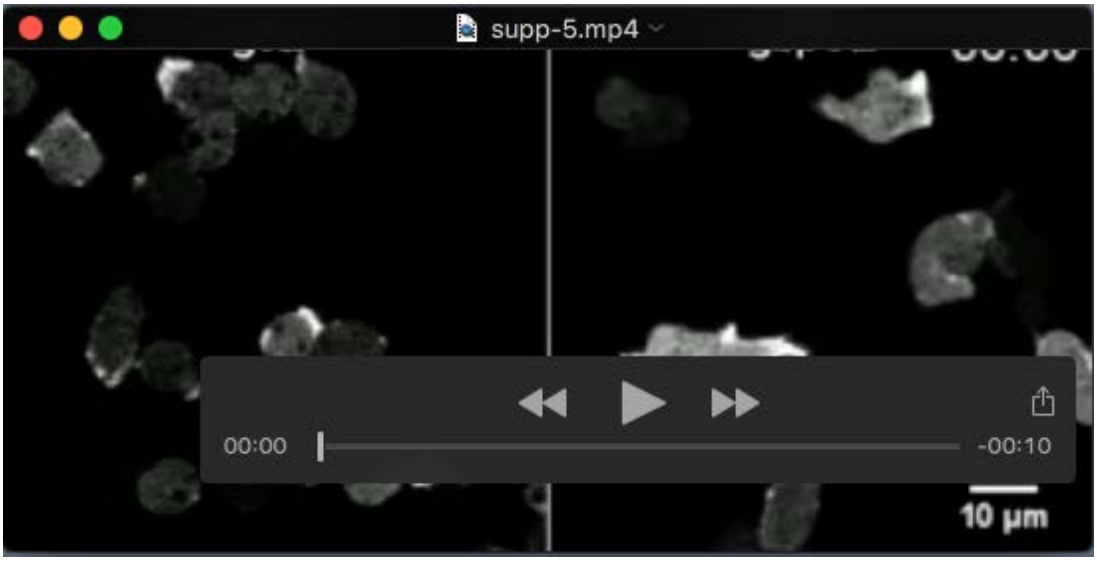

Movie 4. F-actin response in *gcΔ and gbpCΔ* cells.

mRFP-LimEΔcoil-expressing *gcΔ and gbpCΔ* cells were stimulated with 10 nM cAMP. The video was captured every 5 sec and is shown at 12 frame/sec. Time format is "mm:ss".